Eddy shape, orientation, propagation and mean flow feedback in western boundary current jets

Author:
Waterman, Stephanie; Hoskins, B

Publication details:
Journal of Physical Oceanography
v. 43
Chapter No. 8
pp. 1666-1690
0022-3670 (ISSN)

Publication Date:
2013

Publisher DOI:
http://dx.doi.org/10.1175/JPO-D-12-0152.1

Eddy Shape, Orientation, Propagation, and Mean Flow Feedback in Western Boundary Current Jets

STEPHANIE WATERMAN*

Grantham Institute for Climate Change, Imperial College, London, United Kingdom

BRIAN J. HOSKINS

Grantham Institute for Climate Change, Imperial College, London, and Department of Meteorology, University of Reading, Reading, United Kingdom

(Manuscript received 17 August 2012, in final form 12 May 2013)

ABSTRACT

This manuscript revisits a study of eddy–mean flow interactions in an idealized model of a western boundary current extension jet using properties of the horizontal velocity correlation tensor to diagnose characteristics of average eddy shape, orientation, propagation, and mean flow feedback. These eddy characteristics are then used to provide a new description of the eddy–mean flow interactions observed in terms of different ingredients of the eddy motion. The diagnostics show patterns in average eddy shape, orientation, and propagation that are consistent with the signatures of jet instability in the upstream region and wave radiation in the downstream region. Together they give a feedback onto the mean flow that gives the downstream character of the jet and drives the jet's recirculation gyres. A breakdown of the eddy forcing into contributions from individual terms confirms the expected role of cross-jet gradients in meridional eddy tilt in stabilizing the jet to its barotropic instability; however, it also reveals important roles played by the along-jet evolution of eddy zonal–meridional elongation. It is the mean flow forcing derived from these patterns that acts to strengthen and extend the jet downstream and forces the time-mean recirculation gyres. This understanding of the dependence of mean flow forcing on eddy structural properties suggests that failure to adequately resolve eddy elongation could underlie the weakened jet strength, extent, and changed recirculation structure seen in this idealized model for reduced spatial resolutions. Further, it may suggest new ideas for the parameterization of this forcing.

1. Introduction

Understanding the role of eddies and their interaction with the larger-scale flow in western boundary current extension (WBCE) jet systems such as the Gulf Stream and Kuroshio Extensions is critically important because WBCE jets are of fundamental importance to the dynamics of basin-scale circulations and the ocean's global transport of heat, and eddy variability plays a crucial role in WBCE jet dynamics. For example, we expect eddies and their nonlinear interactions to impact mean jet–gyre strength, structure, and stability (Thompson 1978; Dewar and Bane 1989; Hogg 1992; Watts et al. 1995), play a role in driving the jet's flanking recirculations (Hogg 1983, 1985, 1993), couple strong upper-ocean motions to deep abyssal motions (Shay et al. 1995; Howden 2000; Watts et al. 2001), and potentially act as a source of the interannual variability observed in these jet–gyre systems (Spall 1996; Qiu 2000). These effects have important implications for global balances between forcing and dissipation, subtropical–subpolar exchange, the formation of mode water, the transport and storage of heat and potential vorticity (PV), and the steering and intensification of extratropical storms. As such, understanding these effects and their implications is fundamental to our understanding of how ocean basin circulations work and how the ocean plays its role in the climate system.

The problem of understanding the impact of eddies on the larger-scale circulation has modern relevance to

* Current affiliation: Climate Change Research Centre and ARC Centre of Excellence for Climate System Science, University of New South Wales, Sydney, Australia.

Corresponding author address: Stephanie Waterman, Climate Change Research Centre, Level 4, Mathews Building, University of New South Wales, Sydney, NSW, 2052, Australia.
E-mail: snw@alum.mit.edu

DOI: 10.1175/JPO-D-12-0152.1

the representation of eddy effects in global ocean models, which, at present, do not resolve the full extent of the eddy variability. The literature provides compelling evidence suggesting that resolving mesoscale (on the order of 10 km) eddy variability in the ocean component model will significantly impact the simulation of large-scale climate. In WBCE jet regions in particular, explicitly resolving mesoscale eddies results in significantly stronger currents, extended zonal penetration, and associated sharper sea surface temperature fronts and significant structural changes in simulated rainfall (Kirtman et al. 2012). In typical climate models at say 200-km horizontal resolution, eddy features occur on unresolved scales, and there is an important need to parameterize their effects in terms of the resolved variables. Before this can be done however, we must clarify the roles played by the eddy field so that parameterization schemes can be constructed and tested. Understanding the physical mechanisms underpinning eddy effects is critical in parameterization design, as confidence in our projections of future climate for instance relies on correctly representing the dependence of eddy processes on forcings projected to change under future climate changes.

Because of its importance, work on the subject of eddy–mean flow interactions in WBCE jets has a long history, see Waterman and Jayne (2011) for a detailed summary. Much focus (see, for example, Spall 1994; Jayne et al. 1996; Beliakova 1998; Jayne and Hogg 1999; Mizuta 2010) has been on the role of eddies in driving time-mean recirculation gyres in these systems, which add significantly to the WBCE jet transport and play an important role in mode water formation. The study of Waterman and Jayne (2011), on which this present study builds, identified two distinct roles of eddies in the dynamics of the time-mean circulation in an idealized WBCE jet system: that of stabilizing the jet to its barotropic and baroclinic instability, and that of driving the mean recirculations. A key result was identifying the conceptually useful localization of each effect to a distinct along-stream region defined by the stability properties of the time-mean WBCE jet.

This study revisits the examination of eddy–mean flow interactions in an idealized model of a WBCE jet of Waterman and Jayne (2011) from a new perspective, namely through the consideration of average eddy shape, orientation, and propagation characteristics, and the implications of these properties for the eddy effect on the mean flow. By understanding these properties, the physical mechanisms underpinning their distributions, and the roles that they play in determining the eddy feedback effect, it is hoped that new insight into the important eddy–mean flow interactions in WBCE jet systems will be gained.

The outline of this paper is as follows. In section 2, we give a brief description of the idealized WBCE jet model used in the study and provide a summary of our understanding of eddy–mean flow interactions in this configuration from previous work. In section 3, we describe the theoretical background required to define properties of average eddy shape and orientation from terms in the horizontal velocity correlation tensor, and to understand the relationship between these properties and properties of average wave propagation and mean flow feedback effects. Results of this study relate to the application of this framework to the model in a typical WBCE jet–relevant configuration and parameter regime, and are described in sections 4 and 5. In section 4, we describe and interpret properties of the various terms of the horizontal velocity correlation tensor diagnosed from the model and their implications for average eddy shape, orientation, and propagation characteristics. In section 5, we discuss the implications of these distributions on eddy–mean flow feedback effects. We summarize and discuss our results in section 6, considering physical mechanisms that may underpin the eddy effects that are suggested by this new perspective on the eddy forcing, as well as the potential implications of our results. In a companion paper, this understanding is used as the basis for analysis of the breakdown of the eddy feedback effect in this model as spatial resolution is degraded.

2. Model

Our study builds upon a past investigation of eddy–mean flow interactions in the along-stream evolution of an idealized WBCE jet using a numerical model of a zonally evolving, unstable, strongly inertial, boundary-forced jet in an open domain described in full in Waterman and Jayne (2011). In brief, the idealized WBCE jet model we use is quasigeostrophic, on a β plane, and fully nonlinear, with x (zonal), y (meridional), and time dependence. Here we consider only the barotropic, one-layer configuration. The extension of this study to a two- or three-layer system with the addition of baroclinic instability is a topic of future study. The model is forced at the western boundary by imposing a jet inflow directed eastward at $x = 0$ that is scaled appropriate to a WBCE jet. This inflowing jet is potentially barotropically unstable [i.e., it satisfies the Rayleigh necessary condition for instability requiring the meridional gradient of the absolute vorticity $(\partial/\partial y)\zeta_a = \beta - (\partial^2/\partial y^2)U$ to change sign].[1] The instability of the jet provides the only

[1] Here ζ_a is the absolute vorticity, β is the meridional planetary vorticity gradient, and $-(\partial^2/\partial y^2)U$ is the meridional gradient of the jet's relative vorticity $-(\partial/\partial y)U$, where U is the zonal velocity of the inflowing jet.

source of eddy variability in the problem. From $x = 0$ the jet evolves freely in the zonal direction, with the inflowing jet mass removed at the eastern edge of the domain a long way downstream and in a manner that does not affect the upstream dynamics we study. Highly dissipative sponge layers on all the lateral boundaries prevent wave reflection back into the interior to simulate open ocean conditions there. In the interior dissipation is small, such that it is negligible in the time-mean vorticity balance.

We pose the eddy–mean flow interaction problem in terms of a time-mean state and the variability about this mean state. We spin the system up to a statistically steady state (domain-integrated enstrophy is approximately constant with time), then accumulate turbulent statistics for a period long enough so that they are insensitive to the integration time. We consider the problem in nondimensional form in terms of nondimensional variables and dimensional scales L and U, which represent typical horizontal length and velocity scales of the jet, respectively. A dimensional scaling of $L = 40\,\text{km}$ and $U = 1\,\text{m}\,\text{s}^{-1}$ for the typical WBCE jet model run discussed here ($\beta_{\text{nondimensional}} = 0.05$) makes the inflowing jet profile consistent with the velocity and length scales of the Kuroshio jet where it separates from the coast. For further details on the model setup and its relation to observations of the Kuroshio Extension jet, see Waterman and Jayne (2011) and Waterman et al. (2011).

Details on the numerical method can be found in Jayne and Hogg (1999). In brief, integration in time and space is done using a scheme that is center differenced in the two spatial dimensions (an Arakawa A grid) and advective terms are handled using the enstrophy-conserving scheme of Arakawa (1966). At each time step, the relative vorticity is inverted to find the streamfunction using the generalized Buneman algorithm (Adams et al. 1988). The streamfunction is stepped forward in time using a third-order Adams–Bashforth scheme (Durran 1991). The model is damped by bottom friction but results are qualitatively unchanged if horizontal viscosity is used as the dissipation form. For the model run discussed here, we have applied a nondimensional bottom friction coefficient of $R = 1 \times 10^{-6}$, which corresponds to a dimensional dissipation time scale of $O(100$ years).

Previous work using the model has resulted in an understanding of the eddy–mean flow interactions in this configuration that is usefully considered as a two-regime system. See Waterman and Jayne (2011) for a full discussion. In brief, the results reported here are that eddies in this model setup play two distinct roles in their feedback on the time-mean circulation: 1) stabilizing the jet to its instability and 2) driving the time-mean recirculation gyres, with each effect localized to a distinct along-stream region defined by the stability properties of the time-mean jet (Fig. 1). Just after separation from the western boundary, eddies act to stabilize the jet through down-gradient fluxes of vorticity inside the jet and on the jet flanks. A down-gradient flux on the multiple-signed time-mean meridional vorticity gradient of the unstable jet implies a southward eddy vorticity flux in the jet core and northward fluxes on the jet flanks. This pattern results in a four-lobed flux convergence and divergence pattern that drives a circulation that acts to decelerate the jet at its axis and accelerate it on its flanks, in this way stabilizing the jet to its large-scale horizontal shear. Downstream of where the time-mean jet has (through the effect of the eddies) been stabilized, eddies act to drive the time-mean recirculations through the mechanism of an up-gradient vorticity flux. This up-gradient flux is permitted by an eddy enstrophy convergence downstream of jet stabilization, a convergence that results from the generation of eddies in the upstream region where the jet is unstable, the advection of that eddy activity along stream by the jet, and the dissipation of the eddies in the region downstream of jet stabilization. It is in this region of eddy decay that eddies drive the time-mean recirculations through the mechanism of nonlinear eddy rectification, resulting from the radiation of waves from a localized region.

3. Theoretical background

New insights into the eddy feedback effect in this problem come from the application of the ideas presented in Hoskins et al. (1983) in the context of atmospheric eddies, in particular a consideration of the terms of the horizontal velocity correlation tensor and their implications for characteristics of average eddy shape, orientation, propagation, and mean flow feedback. We briefly review these diagnostics here.

Our diagnoses of eddy shape, orientation, propagation, and mean flow feedback all derive from terms of the horizontal velocity correlation tensor $\mathbf{C}_{ij} = \overline{v_i' v_j'}$, where the bar signifies an averaging operator, in this case time averaging, and the prime a deviation from this average. Here, i and j are indices running from 1 to 2 denoting the two horizontal dimensions (zonal and meridional), respectively. It is convenient to separate this symmetric tensor into its isotropic and anisotropic parts such that

$$\mathbf{C} = \begin{pmatrix} \overline{u'^2} & \overline{u'v'} \\ \overline{u'v'} & \overline{v'^2} \end{pmatrix} = \begin{pmatrix} K & 0 \\ 0 & K \end{pmatrix} + \mathbf{A}. \tag{1}$$

Here, the kinetic energy of the eddies $K = 1/2(\overline{u'^2 + v'^2})$. The anisotropic part of the tensor $\mathbf{A}$ is given by

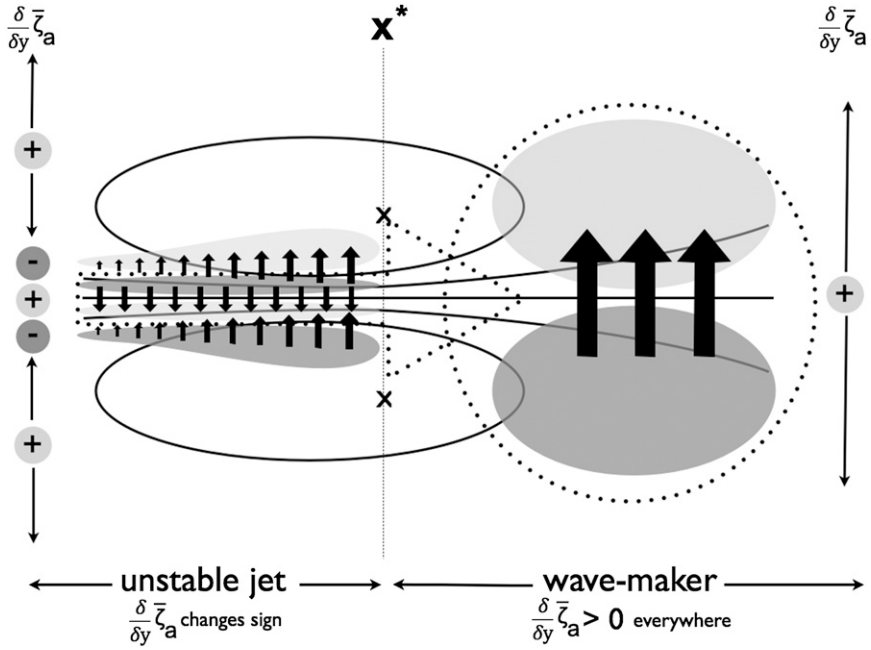

FIG. 1. A summary of the two-regime description of eddy–mean flow interactions in an idealized WBCE jet based on the study of Waterman and Jayne (2011). Solid black lines show a schematic of the time-mean streamlines and illustrate a broadening jet flanked by two time-mean recirculations. Here, and in following figures, various features of the time-mean circulation are indicated for reference: **x** denotes the location of the max time-mean recirculation transport and corresponds in lon with x^*, an along-stream boundary between an upstream ''unstable jet'' region and a downstream ''wave maker'' region defined by the meridional gradient of the time-mean jet's absolute vorticity. Solid black arrows and the filled contours denote the sense of the divergent time-mean eddy vorticity fluxes and the key patterns of their convergence/divergence, respectively. Here, and in following figures, light gray shading indicates positive values (here an eddy vorticity flux convergence) and dark gray shading indicates negative values (here an eddy vorticity flux divergence). Dotted lines denote key features of the advection of eddy enstrophy: a large eddy enstrophy convergence in the downstream region (dotted circle) and the advection of eddy activity from upstream (dotted arrow).

$$\mathbf{A} = \begin{pmatrix} M & N \\ N & -M \end{pmatrix}, \tag{2}$$

with

$$M = 1/2(\overline{u'^2 - v'^2}) \quad \text{and} \quad N = \overline{u'v'}. \tag{3}$$

Familiar from a long history of studies of the effect of eddies on the zonally averaged flow (e.g., Starr 1968), N describes the meridional tilt of eddies/waves that can be interpreted in terms of an elongation either in a ''backward'' or ''forward'' direction depending on its sign (see Figs. 2a,b). Analogously, M describes the second component of a two-dimensional eddy elongation that needs to be considered when one moves from the consideration of the zonally averaged flow to flow with two-dimensional dependence. It should be noted that in axes tilted by an angle of $\pi/4$ (quantities denoted by *), $(M^*, N^*) = (-N, M)$. In this way, M is the equivalent of N for axes tilted by $\pi/4$, and in the original coordinate frame describes the eddy zonal–meridional elongation (Figs. 2c,d).

Consideration of the eddy horizontal velocity covariances cast in terms of K, M, and N is useful because these terms, particularly the latter two, provide information about average eddy shape and orientation, and also about properties of wave propagation and mean flow feedback. In this way, they provide a link between mean flow feedback and eddy structural properties, and as such, may provide physical insight into underpinning mechanisms of the eddy effects.

a. Relation to eddy shape and orientation

The terms K, M, and N can be considered as describing an average or characteristic eddy size, shape, and

orientation at a point.[2] To see this explicitly, we consider the terms of **A** in a coordinate frame aligned with the principal axes of **A** or **C** at angles of $\theta = 1/2 \arctan^{-1}(N/M)$ and $\phi = \theta + \pi/2$ with the x axis. In this frame (quantities denoted by $\hat{}$), $(\hat{M}, \hat{N}) = [(M^2 + N^2)^{1/2}, 0]$. Noting that $\hat{M} = 1/2(\hat{u}'^2 - \hat{v}'^2)$ and $K = 1/2(\hat{u}'^2 + \hat{v}'^2)$ and thus $\hat{M} \leq K$, we define the eddy anisotropy number α as $\alpha = \hat{M}/K$, which describes the characteristic local eddy anisotropy (ellipse eccentricity) as a dimensionless number that lies between 0 and 1. A value of α close to 1 implies that on average eddies are locally extended along the major axis and compressed along the minor axis (i.e., eddies are locally highly anisotropic), whereas a value of $\alpha = 0$ implies $\hat{u}' = \hat{v}'$ and average eddy motions are locally isotropic. The angle θ describes the orientation of the principal axes of **C** and **A** with respect to the basic geographical frame as defined above. It gives information about the average local orientation of the principal eddy variability and hence the local direction of eddy elongation, the degree to which is characterized by α. It also defines the dominant orientation of the local eddy momentum flux.

The parameters α and θ relate instinctively to the description of eddy variability via velocity variance ellipses, a more familiar way in oceanography to illustrate the local principal direction and the degree of anisotropy of the eddy variability as well as the magnitude of the eddy energy [see Morrow et al. (1994); after Preisendorfer (1988) for further details]. In this description, anisotropic eddy variability is represented by an elongated ellipse with the principal direction of the velocity variance aligned with the direction of the ellipse major axis, while isotropic flow is represented by a circular ellipse with zero covariance. The major and minor axes of the ellipse, a and b, are customarily defined in terms of the horizontal velocity correlation tensor components as $a = [\overline{u'u'}\cos^2\theta + \overline{u'v'}\sin(2\theta) + \overline{v'v'}\sin^2\theta]^{1/2}$ and $b = [\overline{u'u'}\cos^2\phi + \overline{u'v'}\sin(2\phi) + \overline{v'v'}\sin^2\phi]^{1/2}$, respectively, where θ and ϕ are as defined above. The velocity variance ellipse major and minor axes can be expressed more simply in terms of the eddy anisotropy and eddy kinetic energy by considering them in the coordinate frame of the principal axes. Then $a^2 = \widehat{\overline{u'^2}} = K + \hat{M} = (1 + \alpha)K$ and $b^2 = \widehat{\overline{v'^2}} = K - \hat{M} = (1 - \alpha)K$.

b. Relation to eddy propagation

As described in Hoskins et al. (1983), in simple situations, the anisotropic velocity correlation tensor can also provide information on the relative propagation of eddy activity. Assuming WKBJ conditions (see, for example, Dingle 1973) of slow mean flow variations and locally sinusoidal waves, in the barotropic case it can be shown that the propagation of eddies relative to the mean flow $\mathbf{c_{gR}}$ is given by

$$\mathbf{c_{gR}} = \mathbf{c_g} - \overline{\mathbf{u}} = \frac{2}{\overline{\zeta'^2}}(-M\overline{\zeta_{ay}} + N\overline{\zeta_{ax}},\ -M\overline{\zeta_{ax}} - N\overline{\zeta_{ay}}). \tag{4}$$

Here $\mathbf{c_g}$ is the intrinsic group velocity of the eddies, $\overline{\mathbf{u}}$ is the time-mean velocity, $\overline{\zeta'^2}$ is the time-mean eddy enstrophy, and $\overline{\zeta_a}$ is the time-mean absolute vorticity. Subscripts denote the spatial derivative in the zonal (in the case of x) and meridional (in the case of y) directions respectively. Equation (4) derives from the Rossby wave dispersion relation for waves whose local streamfunction is $\psi' = A\cos(kx + ly - \omega t)$ and the relations $M/(1/2)\overline{\zeta'^2} = (l^2 - k^2)/(l^2 + k^2)^2$ and $N/(1/2)\overline{\zeta'^2} = -2kl/(l^2 + k^2)^2$, valid if the averaging operator averages the phases of the wave sufficiently. The formulation is useful as it describes how the propagation of eddies/waves relative to the mean flow can be deduced from components of the anisotropic velocity correlation tensor and the spatial gradients of the time-mean vorticity field. In the case where the magnitudes of M and N are comparable and $\overline{\zeta_{ay}} \gg \overline{\zeta_{ax}}$, a condition often satisfied, $\mathbf{c_{gR}}$ is well approximated by $(2/\overline{\zeta'^2})\overline{\zeta_{ay}}(-M, -N)$, offering a simplified description of how the relative propagation of eddies/waves depends on the two components of eddy elongation, M and N, and the background meridional vorticity gradient.

c. Relation to eddy–mean flow feedback

Finally, it is useful to consider the terms of the anisotropic part of the horizontal velocity correlation tensor because the spatial distributions of these terms, and hence the spatial distributions of properties of eddy elongation, determine the eddy–mean flow feedback effect. Note that the symmetric part of the tensor K plays no role in this feedback, just as was the case in the relative propagation. The direct evaluation of the eddy–mean flow feedback, that is, the eddy contribution to the time-mean vorticity budget via the eddy vorticity flux

[2] It is worthwhile to note here that, although the discussion of eddy shape and orientation and the drawing of velocity variance ellipses evoke a mind's eye image of coherent "closed loop" vortex motion, these diagnostics can equally be applied to velocity covariances from other "types" of eddy motion, for example, jet meandering. Also, because properties are diagnosed at a point, they describe local properties which may vary across the scale of a coherent eddy structure. The eddy feedback on the mean flow as defined here depends only on correlation terms at a point/local values of eddy shape and orientation regardless of eddy size or coherence.

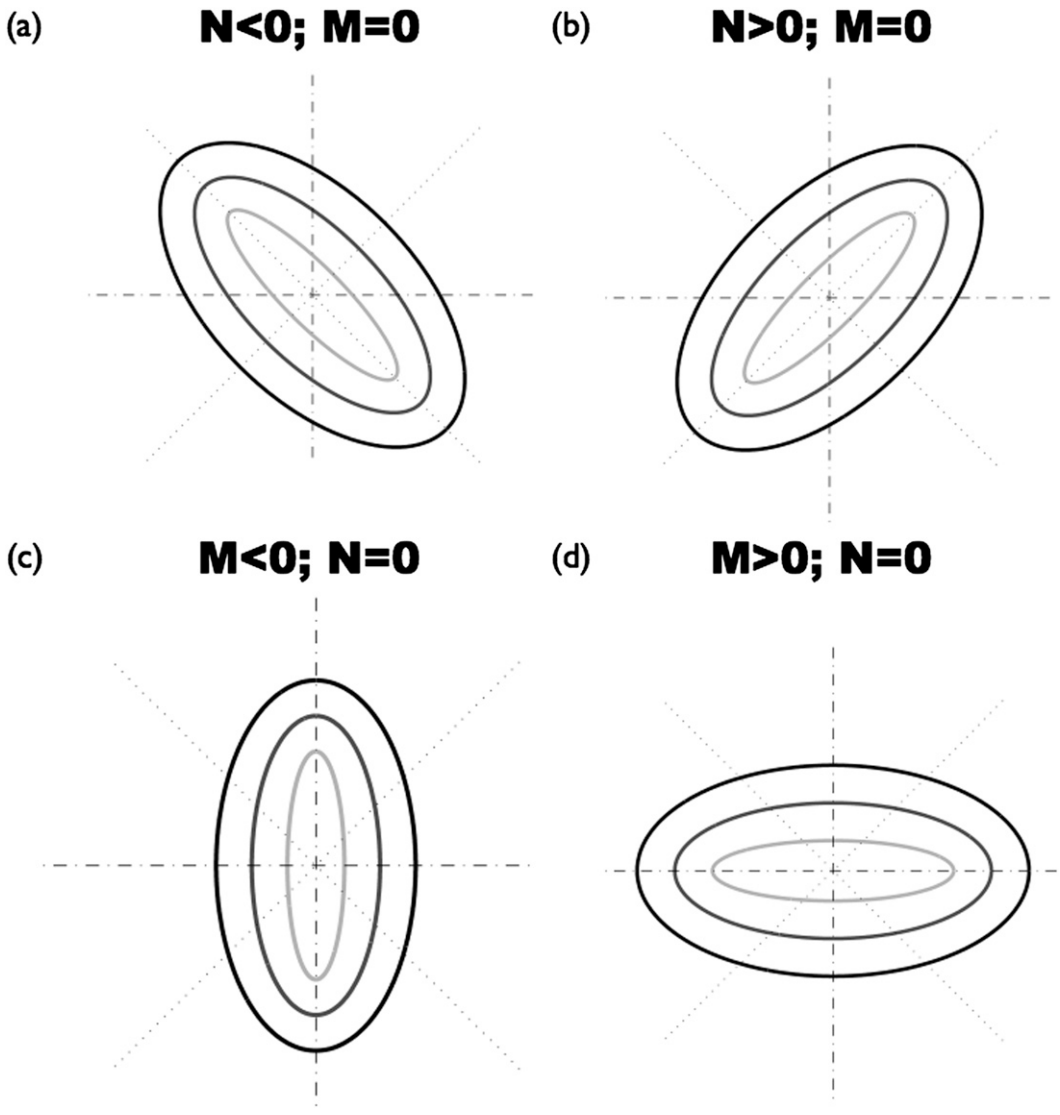

FIG. 2. The interpretation of M and N as describing a generalized two-dimensional eddy elongation in a frame defined by the zonal–meridional directions and a frame rotated by $\pi/4$, respectively. Examples of four characteristic ellipse shapes for the cases of (a) negative and (b) positive values of N (with M zero) and (c) negative and (d) positive values of M (with N zero). In each case, the three ellipses shown correspond to different values of K, with darker shades indicating larger K values.

convergence, can be written in terms of spatial gradients of M and N as

$$-\nabla \cdot \overline{\mathbf{u}'\zeta'} = 2M_{xy} - N_{xx} + N_{yy}. \tag{5}$$

The impact of the spatial distributions of eddy elongation on eddy–mean flow feedback can also be considered more simply under the approximation that N_{xx} can be neglected. This is valid if the zonal scale of N is much larger than its meridional scale, which is often the case, and will be shown to be valid here. In this case, the mean flow vorticity forcing is well approximated by the meridional derivative of the divergence of the so-called "E vector" $\mathbf{E}$:

$$-\nabla \cdot \overline{\mathbf{u}'\zeta'} \simeq 2M_{xy} + N_{yy} = -\frac{\partial}{\partial y}(\nabla \cdot \mathbf{E}), \tag{6}$$

where $\mathbf{E} = -(2M, N)$.

Hoskins et al. (1983) argue that the divergence of the E vector field gives the sense of the eddy-forced mean circulation, and it can be helpful in the atmospheric context to consider the divergence of $\mathbf{E}$ as an equivalent eddy forcing of mean zonal momentum, F^x. The

contribution of such a force to the forcing of mean vorticity would be $-(\partial/\partial y)F^x$, and comparing with Eq. (6) shows that it is valid to take $F^x = \nabla \cdot \mathbf{E}$. We point out here that this is helpful when the mean flow dynamics are dominated by zonal advection, such as in an atmospheric storm track. However, in large-scale steady oceanographic situations, in which time-mean absolute vorticity advection is often dominated by the meridional advection of planetary vorticity, it is likely to be preferable to consider the mean vorticity balance in which $-\partial/\partial y(\nabla \cdot \mathbf{E})$ is balanced by a mean planetary vorticity flux, that is,

$$\beta\overline{v} = -\frac{\partial}{\partial y}(\nabla \cdot \mathbf{E}). \tag{7}$$

We will see that in the present application, this balance with the mean meridional motion is important in weaker mean flow regions.

We note the relation between the direction of **E**, that of $-(2M, N)$, and that of the relative eddy propagation, in particular for the case when the mean absolute vorticity contours make only small angles with the zonal direction such that the latter can be approximated as $-(M, N)$. In this case, the orientation of $\mathbf{c_{gR}}$ and **E** are closely related. They are identical when M or N is zero, and quite generally in the same quadrant in (x, y) space but with **E** being more zonal. In this way, the eddy circulation forcing is related to the divergence of a vector field closely related to that of eddy propagation. Consideration of the eddy forcing in the E vector framework also has the key advantage over consideration of the eddy vorticity flux convergence of being dependent on only first, as opposed to second, derivatives of M and N. These are inherently less noisy, and make the task of linking spatial patterns of eddy elongation to the eddy forcing more straightforward. In both cases, formulating the eddy forcing in terms of M and N is useful as it allows an understanding of how the eddy-forcing effects arise as a consequence of the spatial distributions of eddy structure, enabling insights into eddy behavior and feedbacks.

4. K, M, and N and their implications for eddy shape, orientation, and propagation

We now examine the fields of K, M, and N that compose the horizontal velocity correlation tensor for the idealized WBCE jet configuration. It is found that they exhibit systematic patterns in their spatial distributions, in particular with respect to their evolution along the jet axis and to regime boundaries defined by the time-mean jet's stability boundary x^* and the along-stream location of the maximum in eddy kinetic energy (EKE) $x^{\mathrm{EKE\ max}}$ (Fig. 3).[3] As seen in Fig. 3a, K increases along the jet axis with along-stream distance to $x^{\mathrm{EKE\ max}}$ and decays further downstream. The broad distribution of elevated EKE around a downstream maximum value is consistent with wave radiation from the jet downstream of x^*. As seen in Fig. 3b, M has a region of positive values (zonal elongation) with local maxima on the jet flanks far upstream ($x < x^*$) and a region of negative values (meridional elongation) far downstream ($x > x^{\mathrm{EKE\ max}}$). In between these there is a "bullet" of negative M (meridional elongation) on the jet axis in the vicinity of x^*, a region where instability signatures are maximized, and a region of large positive values near $x^{\mathrm{EKE\ max}}$. The latter is consistent with the existence of an effective wave radiator centered on the jet axis just downstream of $x^{\mathrm{EKE\ max}}$, with westward relative propagation to the west of it and eastward propagation to the east. Figure 3c shows that N is characterized by signatures typical of barotropic instability in the upstream unstable jet region ($x \leq x^*$): N large and positive on the flanks of the jet to the north of the jet axis and large and negative on the flanks of the jet to the south of the jet axis, indicating eddy tilts against the shear consistent with them extracting energy from the mean flow. The reverse pattern downstream ($x \geq x^*$), a broad distribution of negative N to the north of the jet axis and positive N to the south of the jet axis, is consistent with wave radiation from the jet. Inside the jet, M tends to dominate over N so that eddies tend to be oriented zonally or meridionally, and the sign of M indicates eddy orientation and propagation. In the far field, the magnitudes of M and N tend to be comparable but with the latter slightly larger.

These distributions of the terms of the horizontal velocity correlation tensor imply systematic patterns in eddy shape and orientation. As seen in Fig. 4a, the eddy anisotropy number α implies that inside the jet eddies are, on average, locally highly anisotropic in the upstream region, particularly on the flanks of the jet. The pattern is consistent with the signature of zonal motions dominating near the northern and southern edges of strongly titled eddies that may extend in a banana shape across the unstable jet axis. Eddies become more circular with downstream distance until the vicinity of x^* and $x^{\mathrm{EKE\ max}}$, where eddy anisotropy is small. Eddies are increasingly locally anisotropic with further distance downstream

[3] Specifically x^* is defined by the zonal location of maximum time-mean recirculation transport found to coincide approximately with the zonal location where the time-mean meridional absolute vorticity gradient first ceases to change sign across the jet, that is, where the time-mean jet is first necessarily stabilized to its barotropic instability. See Waterman and Jayne (2011) for further details.

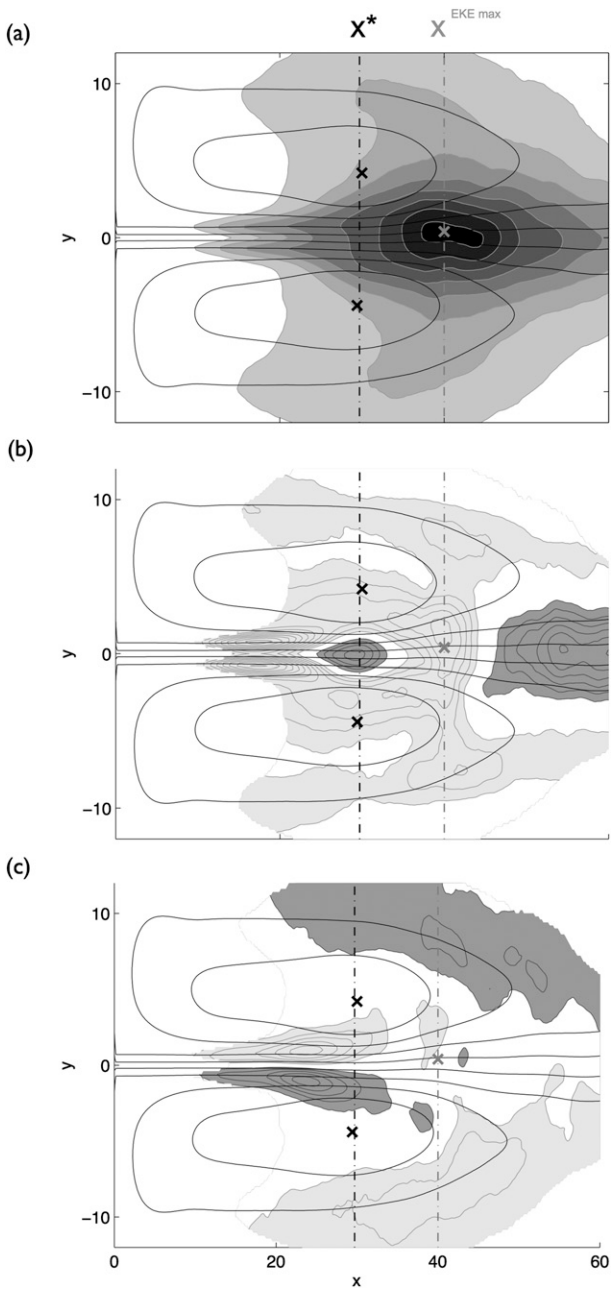

FIG. 3. Visualization of the terms that compose the horizontal velocity correlation tensor in an idealized WBCE jet model: (a) K, (b) M, and (c) N. Contours are drawn in intervals of 0.01, 0.002, and 0.0025 nondimensional units, respectively, and are shown only where K exceeds the critical value of 0.01 nondimensional units. In all panels and in following figures $x^{\mathrm{EKE\ max}}$, the location of the max EKE, is indicated by the gray boldface x. The vertical dashed gray line indicates the along-stream location of $x^{\mathrm{EKE\ max}}$.

and distance from the jet in the far field. From Fig. 4b that gives eddy orientation θ, it is seen that inside the jet and on its flanks, eddies are, on average, locally oriented zonally in the upstream region ($x < x^*$) and meridionally downstream ($x > x^{\mathrm{EKE\ max}}$). There is additional structure in the vicinity of x^* and $x^{\mathrm{EKE\ max}}$ where eddies are meridionally and zonally elongated, respectively, consistent with the values of M and N, but the small anisotropy of the eddies in these regions should be recalled. Outside the jet, the eddy orientations mostly reflect the sign of N. In the upstream region, eddies are tilted "into the jet," a northeast–southwest orientation to the north of the jet and a northwest–southeast orientation to the south of the jet. In the far field, the tilt is the reverse, a northwest–southeast orientation to the north of the jet and a northeast–southwest orientation to the south of the jet. As noted in the description of N, the signatures upstream and at x^* are consistent with barotropic instability, while the downstream and far-field patterns are consistent with wave radiation from the jet.

Aspects of the implied wave propagation have already been introduced but will now be considered in a more complete manner. Figures 5a,b give the magnitude and direction, respectively, of the absolute group velocity implied by these patterns of M and N, the time-mean absolute vorticity gradients, and the time-mean velocity obtained using Eq. (4). Figure 5b also includes the direction of the relative group velocity, while Fig. 5c shows the relative magnitude and direction of the zonal component of the relative group velocity, the time-mean velocity and the absolute group velocity along the jet axis. The group velocity on the jet axis goes through zero at the zonal location indicated $x^{c_{gx}=0}$ with absolute propagation inside the jet being upstream of this location and downstream of this point. In the far-upstream region $x < x^{c_{gx}=0}$, the magnitude of the group velocity is large, and absolute propagation is upstream on the jet axis and downstream and away from the jet axis on the jet flanks. In the region of the instability bullet ($x \sim x^*$) it is eastward and toward the jet axis on the jet flanks. Downstream of this is the radiator region with propagation away from an effective wave radiator located just downstream of $x^{\mathrm{EKE\ max}}$ in all directions: westward on the jet axis to the west, eastward to the east, and away from the axis in all regions to the north and south. Inside the jet, the relative wave propagation mostly dominates over the mean flow. In the far field, the mean flow is more important but the relative propagation is usually of larger magnitude. One important exception is inside the recirculations, where the intrinsic wave speed is negligible and the absolute propagation is effectively that of the mean flow.

It should be recalled that diagnosis of wave propagation via Eq. (4) is strictly valid for small amplitude, neutral waves on a slowly varying flow. Further, it neglects the impacts of instability and nonlinearity. It is therefore worth considering the validity of these results and their

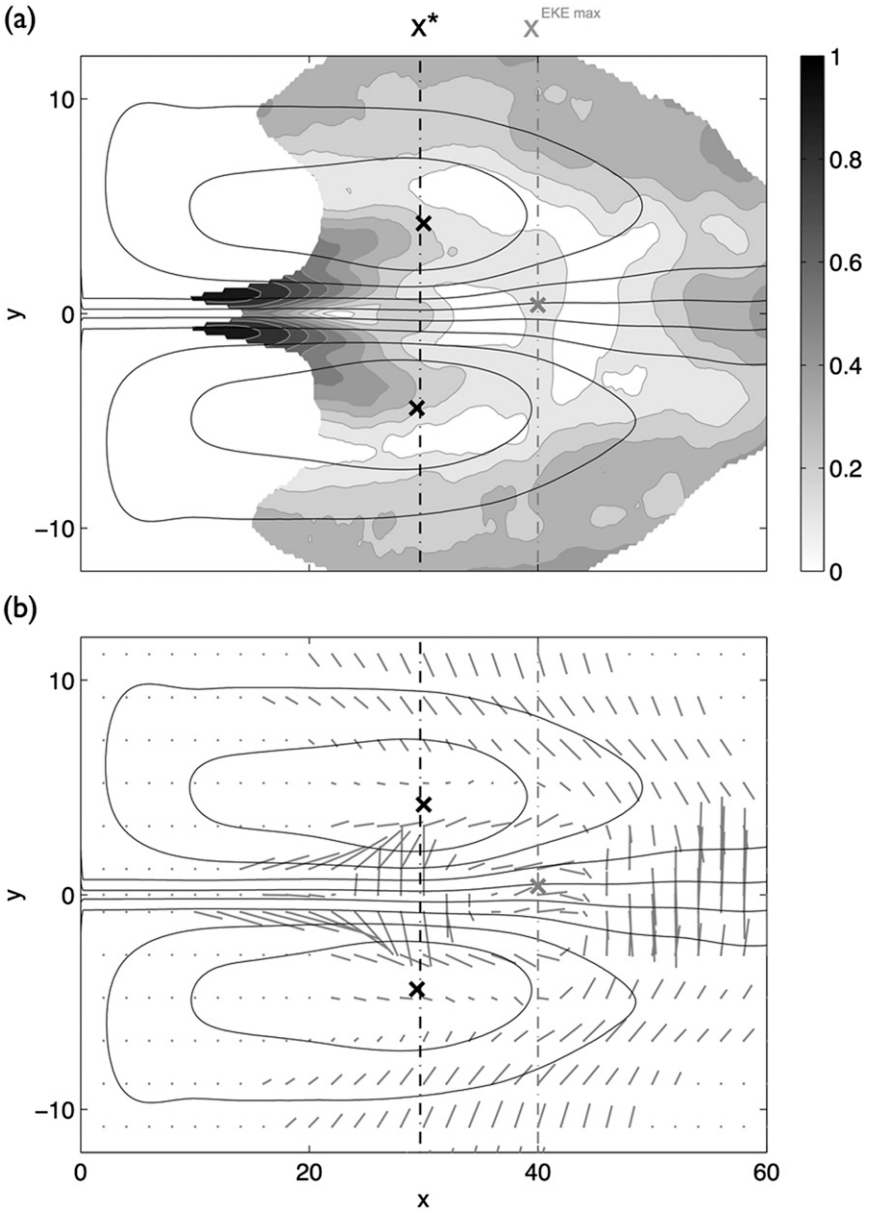

FIG. 4. The spatial distributions of (a) average eddy shape visualized via the eddy anisotropy number α and (b) average eddy orientation θ as defined section 3. In panel (b), vectors are of length $\hat{M} = \sqrt{M^2 + N^2}$ and are oriented at an angle θ from the geographical zonal axis. As in Fig. 3, values are shown only where K exceeds the critical value of 0.01 nondimensional units.

possible implications in the far-upstream jet region where the instability of the flow and the growth of eddies might lead to question the validity of the theory. Confidence in its utility, however, does come from the observation that waves, for which the relative zonal phase speed is much greater than the imaginary phase speed, as is the case here, are often dominated by their neutral mode behavior in many aspects (see, for example, Throncroft et al. 1993). Perhaps more serious is the reality that here the latitudinal scale of the jet with its reversal in its absolute vorticity gradient is very small, and the eddy meridional scale is likely to be similar or even greater. Again, however, other studies have shown that the theory gives good guidance even when the mean flow and eddy scales are comparable (see, for example, Simmons and Hoskins 1979; Throncroft et al. 1993). To give an indication of the possible importance of this problem, Fig. 6 shows various estimates of the absolute

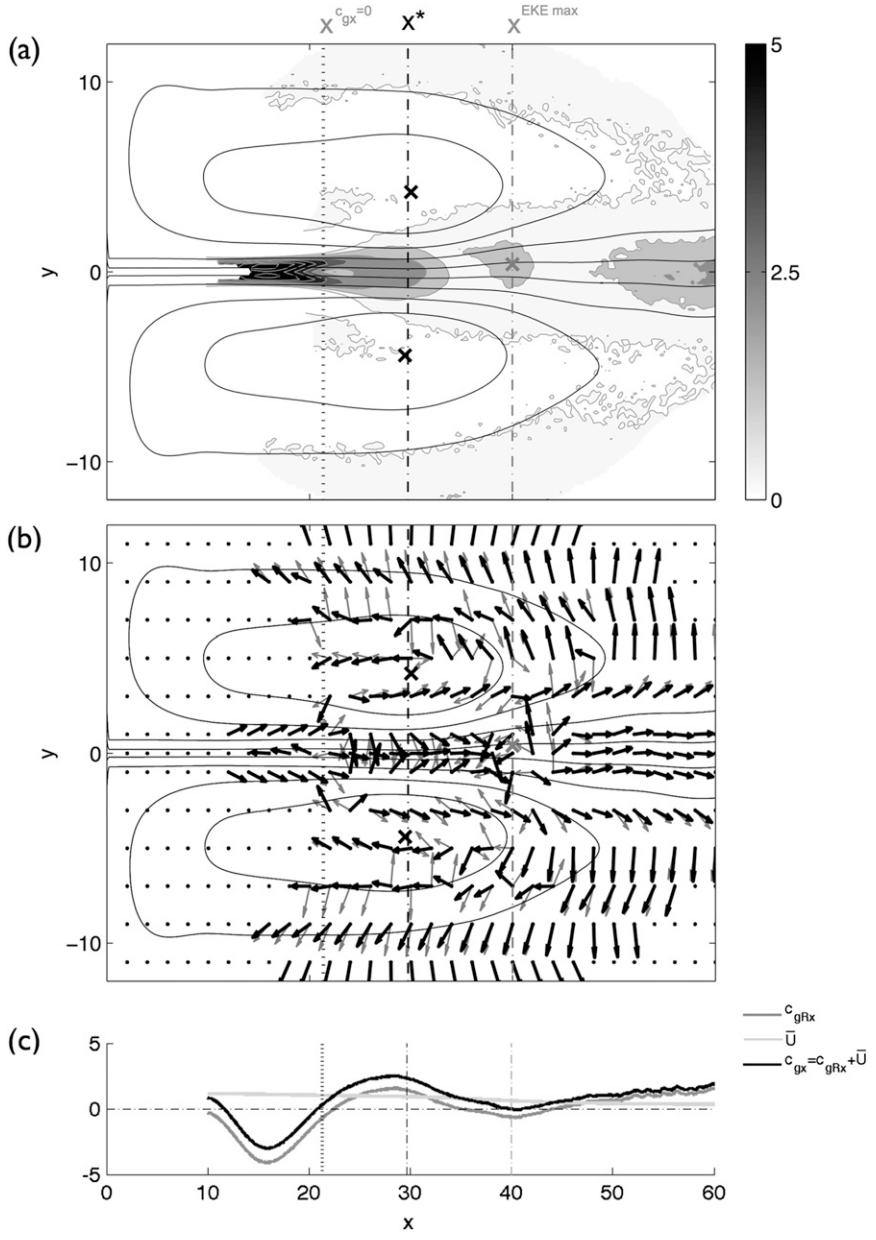

FIG. 5. A characterization of the propagation of eddy activity $\mathbf{c_g} = \mathbf{c_{gR}} + \bar{\mathbf{u}}$ as defined in section 3. (a) The magnitude of the absolute eddy speed, abs($\mathbf{c_g}$). Contours are drawn in intervals of 1 nondimensional unit and shown only where $K > 0.01$. (b) The direction of the relative eddy propagation (gray) and the absolute eddy propagation (thick black). (c) The zonal component of the relative eddy propagation c_{gRx}, the time-mean flow $\bar{u}$, and the absolute eddy propagation $c_{gx} = c_{gRx} + \bar{u}$ along the jet axis ($y = 0$) as indicated in the legend.

group velocity along the jet axis given by Eq. (4) for a range of averaging scales in the meridional direction. It is clear that the eddy shape in this region gives the possibility of group velocities of meridionally coherent eddies that are near zero and even negative. This is consistent with zonally elongated wave activity not being swept downstream by the strong jet and the continued presence of zonally elongated eddy activity in this region.

A summary of the eddy shape and propagation features discussed in this section is presented in the schematics in Fig. 7. Figure 7a highlights the strongly against shear–tilted eddies in the upstream jet and the move toward isotropy downstream but with slight meridional elongation

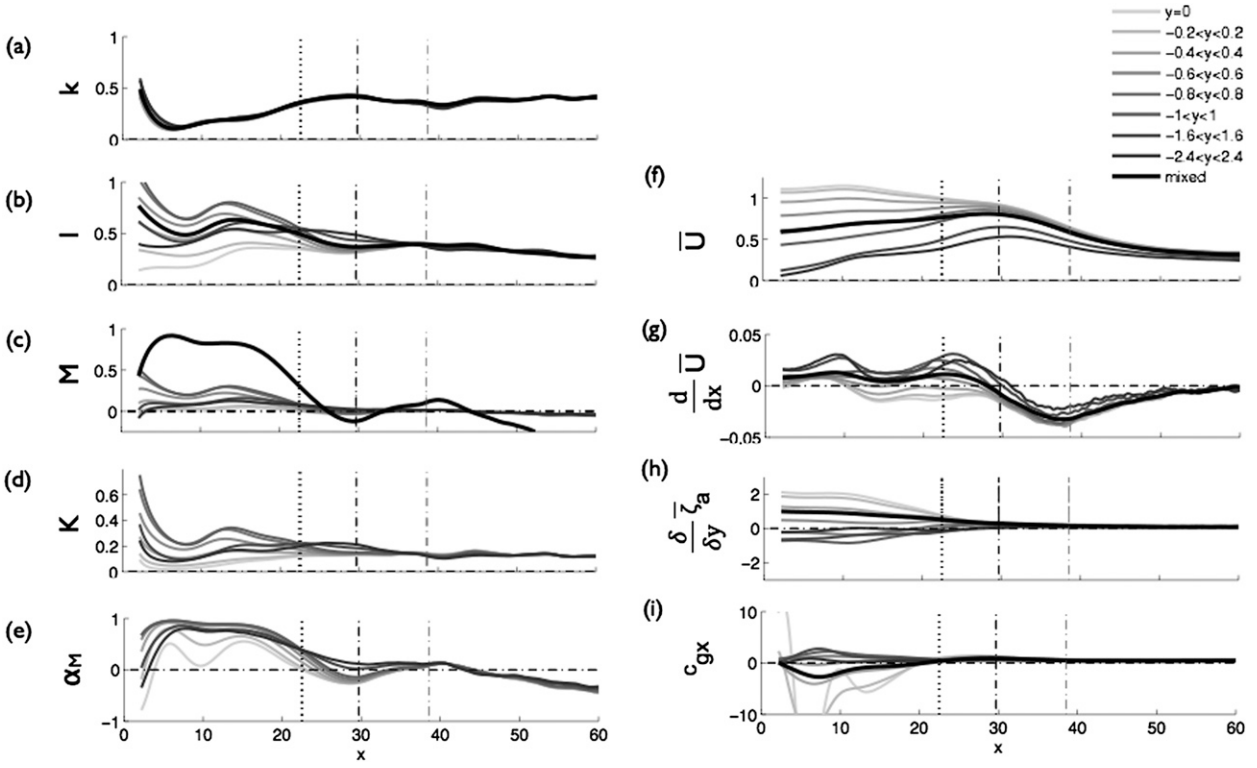

FIG. 6. Along-jet distributions of key quantities along the jet axis and their sensitivity to the choice of the meridional averaging scale. The zonal distributions of the time-mean (a) k and (b) l wavenumbers diagnosed from the ratios of time-mean eddy covariances as $k \sim \sqrt{\overline{v'v'}/\overline{\psi'\psi'}}$ and $l \sim \sqrt{\overline{u'u'}/\overline{\psi'\psi'}}$; (c) M and (d) K computed as $M = 1/2(l^2 - k^2)$ and $K = 1/2(l^2 + k^2)$, respectively; (e) a time-mean eddy elongation number $\alpha_M = M/K$ equal in magnitude to the time-mean eddy anisotropy number along the jet axis (where $N = 0$) and with a sign reflecting the sign of M (and whether elongation is in the zonal or meridional direction); (f) the time-mean zonal velocity $\overline{\mathbf{u}}$; (g) the time-mean zonal velocity zonal gradient $d\overline{\mathbf{u}}/dx$; (h) the meridional gradient of the time-mean absolute vorticity $\partial\overline{\zeta_a}/\partial y$; and (i) the absolute zonal eddy group velocity $c_{gx} = c_{gRx} + \overline{\mathbf{u}}$ derived from the above quantities. Different shades of line denote different meridional averaging intervals as indicated in the legend each which can be considered as legitimately defining the ''along jet'' properties. The mixed range consists of the use of different latitudinal ranges for the averaging of the wavenumber and mean zonal flow derived quantities *vs*. the meridional gradient of absolute vorticity (over $-2 < y < 2$ in the case of the former and $-0.8 < y < 0.8$ in the case of the latter) chosen to capture the jet acceleration in the upstream region but not the negative lobes of the $\partial\overline{\zeta_a}/\partial y$ profile. The need to use different meridional averaging ranges to capture both the zonal acceleration of the upstream jet and the upstream region's upstream wave propagation, exposes the complication that the jet is not slowly varying in the meridional direction compared to the scale of the wave in this direction.

in the instability bullet and zonal elongation near the maximum in K. Downstream of this, the meridional elongation becomes larger with downstream distance. Off the axis away from the unstable region, the tilt is with the ambient shear of the jet. Figure 7b shows the tendency for upstream propagation on the axis of the upstream jet, convergence upstream of $x^{\mathrm{EKE\ max}}$, and radiation away from the radiator region.

5. Implications for eddy–mean flow feedback effects

As discussed in section 3, spatial derivatives of the two components of eddy elongation, M and N, determine the mechanical feedback of the eddies onto the mean flow. Here we consider various diagnostics of eddy-forcing effects, and in each examine the individual contributions coming from the spatial patterns of M and N to understand their respective influence.

a. The eddy vorticity forcing

Figure 8 gives the total eddy vorticity flux convergence, $-\nabla \cdot \overline{\mathbf{u}'\zeta'} = 2M_{xy} - N_{xx} + N_{yy}$, and the contributions of the three component terms on the right-hand side, respectively.

The total vorticity flux convergence (Fig. 8a) shows the upstream ($x \leq x^*$) pattern of negative and positive regions about the axis of the jet, flanked by weaker features of the opposite sign. These are the expected signatures of barotropic instability and down-gradient

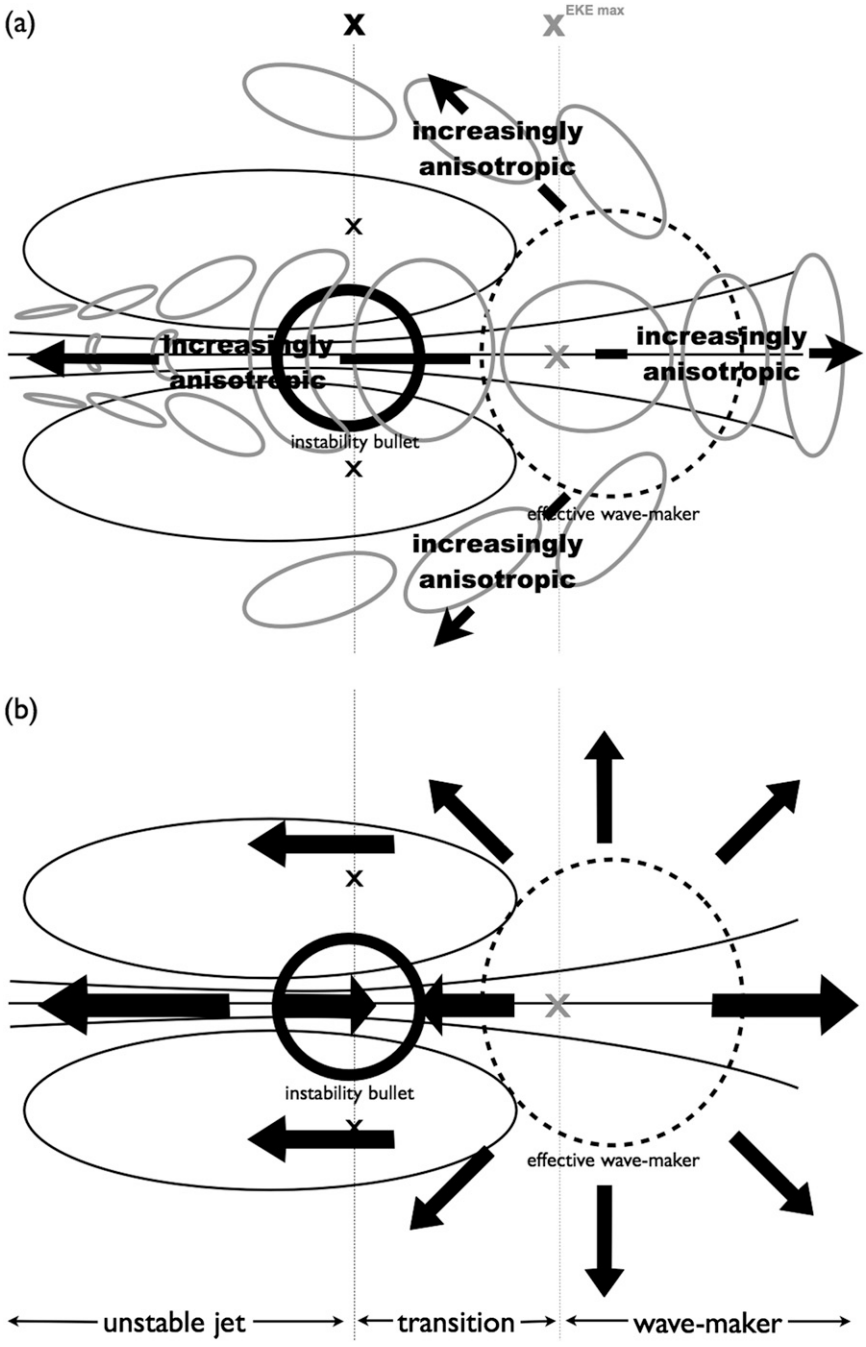

FIG. 7. Schematic summaries of the spatial patterns of (a) eddy shape and orientation and (b) wave propagation, and their relation to key features of the time-mean circulation and conceptualizations of the workings of the system.

vorticity fluxes on a strong positive meridional vorticity gradient in the jet and negative meridional vorticity gradients on the flanks. However, there is additional zonal structure in this pattern, and the dipole around the jet continues and broadens downstream of the unstable region ($x^* \leq x \leq x^{\mathrm{EKE\ max}}$). At $x^{\mathrm{EKE\ max}}$, there is a rapid transition to a broad-scale reversed pattern with a flux convergence to the north of the jet axis and a flux divergence to the south.

Now consider the individual contributions of each of the three component terms that together make up the full eddy forcing. Figure 8c shows that the contribution

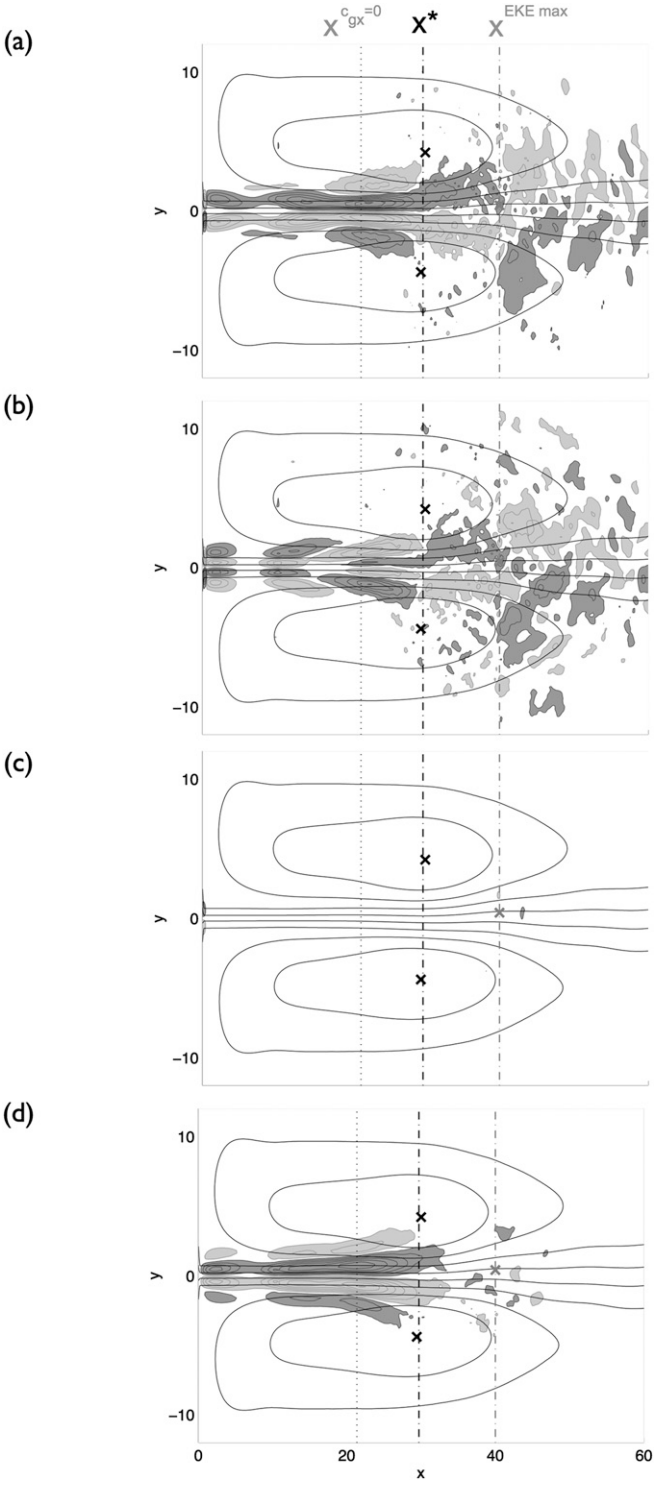

FIG. 8. The relative contributions of the patterns of M and N to the eddy forcing of the mean flow described by (a) the full eddy vorticity flux convergence, $-\nabla \cdot \overline{\mathbf{u}'\zeta'} = 2M_{xy} - N_{xx} + N_{yy}$, and the relative contributions of the individual terms (b) $2M_{xy}$, (c) N_{xx}, and (d) N_{yy}. Contours are drawn in intervals of 0.0025 nondimensional units in all panels. We disregard the interpretation of forcing patterns upstream of $x = 10$ because of the strong influence of sponge layer effects.

of the N_{xx} term is indeed negligible everywhere as expected because the zonal length scale of N is much larger than its meridional scale. We see that the N_{yy} term (Fig. 8d) dominates in the upstream unstable region and gives the quadrupole pattern centered around the y axis. However, the contribution from the M_{xy} term (Fig. 8b) plays an important role throughout the domain. In the upstream unstable region, it acts to modulate and generally slightly reduce the impact of N. However, it is also responsible for the zonal extension up to $x^{\mathrm{EKE\ max}}$ of the signature of down-gradient vorticity flux across the jet. Thus, it acts to extend the region in which wave activity grows and the mean jet weakens beyond that in which a simple barotropic instability criterion would suggest this behavior. Beyond $x^{\mathrm{EKE\ max}}$, the broad cyclonic mean flow forcing to the north of the jet and anticyclonic forcing to the south of the jet are due solely to the M contribution.

It is of interest to consider what aspects of the structure of M and hence the zonal or meridional elongation characteristics of the eddies lead to the structure of its contribution to the total vorticity flux convergence. The far up- and downstream eddy characteristics are strong zonal elongation on the jet flanks (with localized maxima in the vicinity of $x^{c_{gx}=0}$) and meridional elongation inside the jet, respectively. The former gives rise to a quadruple vorticity flux convergence pattern upstream of $x^{c_{gx}=0}$ [the cross-jet gradient of peak M_x values off the jet axis gives rise to a $(M_{xy} > 0)$–$(M_{xy} < 0)$–$(M_{xy} > 0)$–$(M_{xy} < 0)$ quadrupole pattern centered on the jet axis] that acts to weaken the impact of N in the far-upstream region. The latter gives rise to the broad cyclonic and anticyclonic forcing in the downstream region [the cross-jet gradient of a negative M_x value centered on the jet axis gives rise to the $(M_{xy} < 0)$–$(M_{xy} > 0)$ dipole pattern that characterizes the downstream region]. The existence of meridional elongation ($M < 0$) in the instability bullet near x^* upstream of zonal elongation ($M > 0$) to the west of the effective wave maker near $x^{\mathrm{EKE\ max}}$ gives a positive M_x value in the transition region ($x^* < x < x^{\mathrm{EKE\ max}}$), the meridional gradient of which produces the opposite-signed vorticity flux convergence dipole pattern to that further downstream that is responsible for the extension of the down-gradient vorticity flux signature beyond x^*.

b. Mean flow driving by the eddy forcing

The mean circulation–driving effects of this eddy forcing and the individual contributions from M and N are now diagnosed through a series of eddy-forcing experiments, in which the eddy forcing in the form of the eddy vorticity flux convergence or the individual contributions to this total convergence from M or N, are prescribed as an explicit vorticity forcing term on the right-hand side of the model's governing equation. At the same time, intrinsic eddy growth associated with the inflowing jet is damped in the model so that the eddy forcing is due to the prescribed right-hand side forcing alone. See appendix A for further details.

A comparison of the time-mean circulation driven by a prescribed eddy forcing consisting of the individual contributions from M_{xy} versus N_{yy} is shown in Fig. 9. Consistent with the inferences above, here we see that the upstream eddy stabilizing effect consisting of the driving of a pair of narrow cells inside the jet (an anticyclonic cell to the north of the jet axis and a cyclonic cell to the south) with associated deceleration of the jet at its axis and acceleration on its flanks arises primarily from the cross-jet gradients in N (N_{yy}). Again this is consistent with our expectation for the role of eddies in stabilizing the jet to its barotropic instability. The response is somewhat downstream of the forcing as a result of mean flow advection.

As seen in Fig. 9a, upstream of $x^{c_{gx}=0}$, gradients in M (M_{xy}) have a counter-stabilizing effect, acting to sharpen the jet by decelerating it on its flanks. Downstream of $x^{\mathrm{EKE\ max}}$, gradients in M are responsible for driving broad gyres, which also contribute to the acceleration on the flanks of the broad jet in the far downstream region ($x > x^{\mathrm{EKE\ max}}$). In both of these ways, eddy forcing from M acts to extend the strong jet further downstream. In the vicinity of x^*, forcing from M acts to drive meridional motions, while between x^* and $x^{\mathrm{EKE\ max}}$, M extends the stabilizing effects of N further downstream. Worthy of note is that consistent with the observation that M contributions dominate the eddy vorticity forcing in the downstream wave radiator region, the eddy-driven mean flow downstream of x^* and the time-mean recirculations arise in these experiments almost exclusively from the M contribution to the eddy forcing.

c. Eddy forcing from an E vector consideration

Next, we consider the eddy forcing and the relative roles played by M and N through consideration of the divergence of the E vectors as described in section 3c.

Figures 10a and 10b present the magnitude and direction of the E vectors in this configuration, respectively. The magnitudes are large in the upstream region ($x < x^*$) on either side of the jet axis, in the instability bullet in the vicinity of x^*, and near $x^{\mathrm{EKE\ max}}$ and far downstream. They are significant in the whole wave radiation region. The E vector is oriented upstream and toward the jet axis in the upstream region, but elsewhere generally away from the radiator region. Comparison with Fig. 5b shows that there is a notable similarity between the E vector orientation and that of the group velocity, as anticipated from the theoretical discussion in section 3.

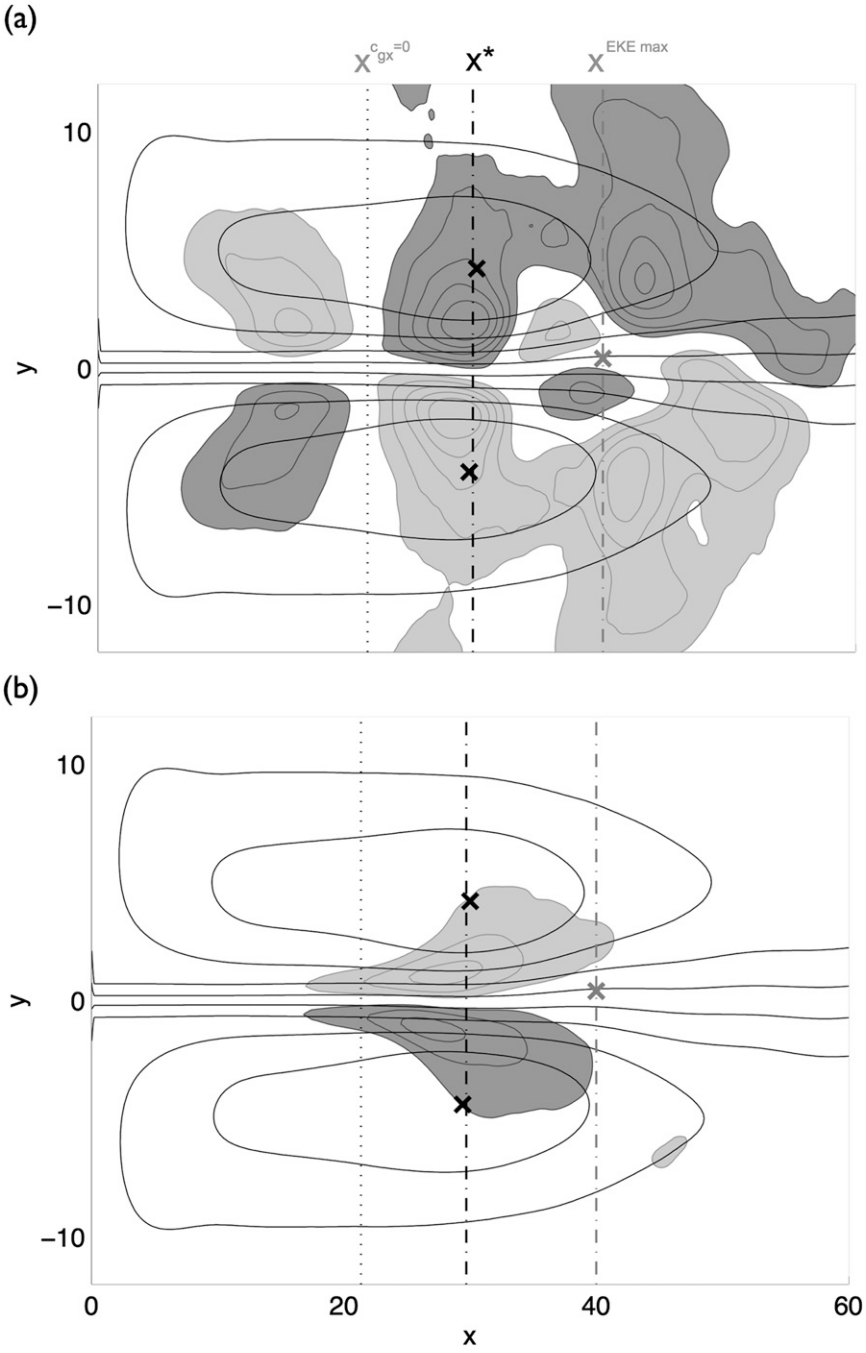

FIG. 9. A visualization of the individual mean flow forcing effects of the contributions from M and N to the eddy vorticity flux convergence via visualization of the eddy-driven component of the time-mean streamfunction (the difference between the forced and unforced time-mean streamfunctions in damped model runs; filled contours) in two eddy forcing experiments forced by (a) $2M_{xy}$ and (b) N_{yy}, respectively. Contours are drawn in intervals of 0.1 nondimensional units in both panels. Properties of the time-mean streamfunction and time-mean EKE distribution overlaid are those from the standard (undamped and unforced) run from which the eddy forcing is diagnosed.

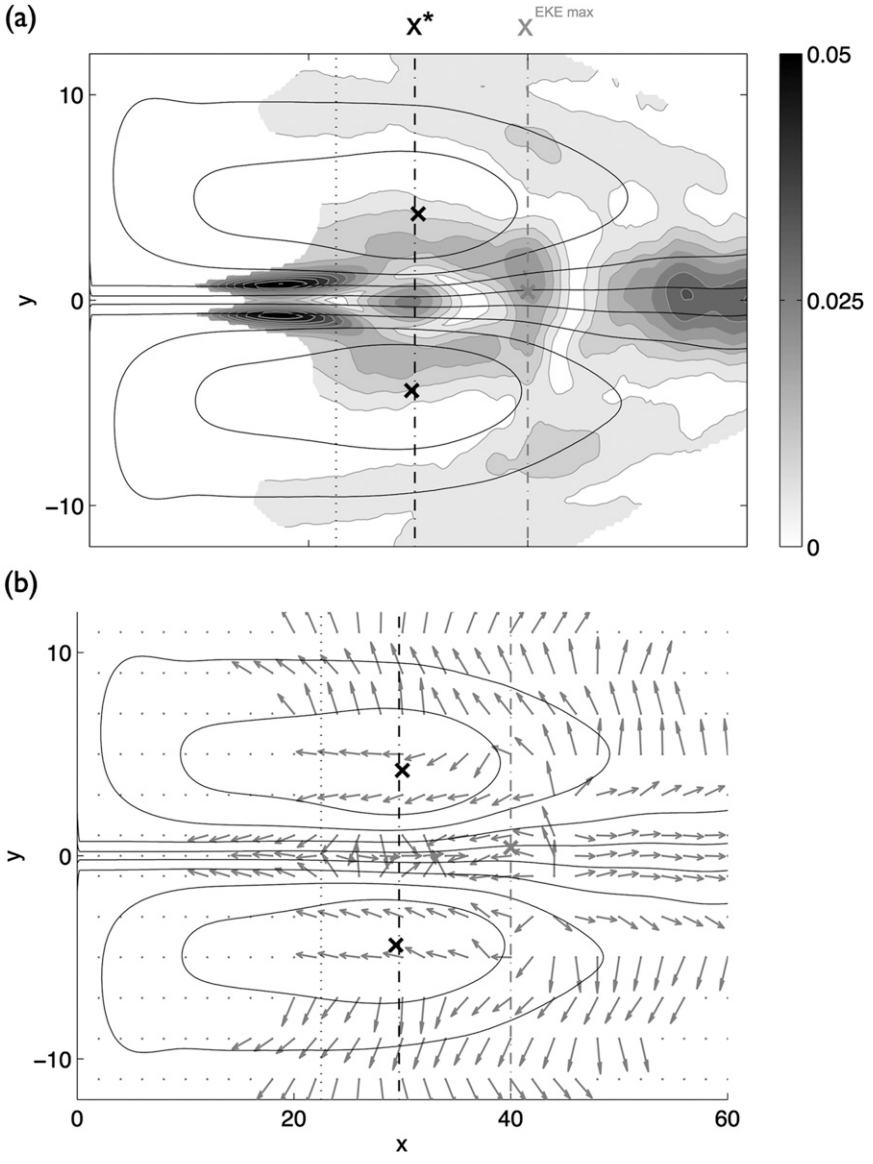

FIG. 10. A characterization of the system's E vectors as defined in section 3. E vector (a) magnitude and (b) direction. Contours in (a) are drawn in intervals of 0.005 nondimensional units.

Figure 11 gives the E vector divergence and the individual contributions to that divergence from M and N. The total divergence (Fig. 11a) shows in the unstable region strong convergence on the jet axis and weaker divergence on either flank, with the convergence extending to $x^{\mathrm{EKE\ max}}$ and broadening. Downstream of this is a broad region of divergence. These features can all be visualized from the magnitude and direction of the E vectors given in Fig. 10. In the upstream region of large zonal mean flow advection, the interpretation of this field in terms of reducing the mean flow on the jet axis and increasing it on the jet flanks is valid. In the downstream region of weaker mean flow, the interpretation in terms of the eddy–mean flow vorticity generation being balanced by the βv term as described by Eq. (7) is more appropriate. As such the E vector divergence weakening with latitude is here interpreted as forcing the meridional component of the recirculation flow.

Figures 11b and 11c give the M and N contributions to the E vector divergence, respectively. Consistent with the conclusions drawn from eddy-forcing experiment results shown in Fig. 9, N is seen as providing the signature consistent with an eddy stabilization effect, which is modulated and reduced by M. However M extends the

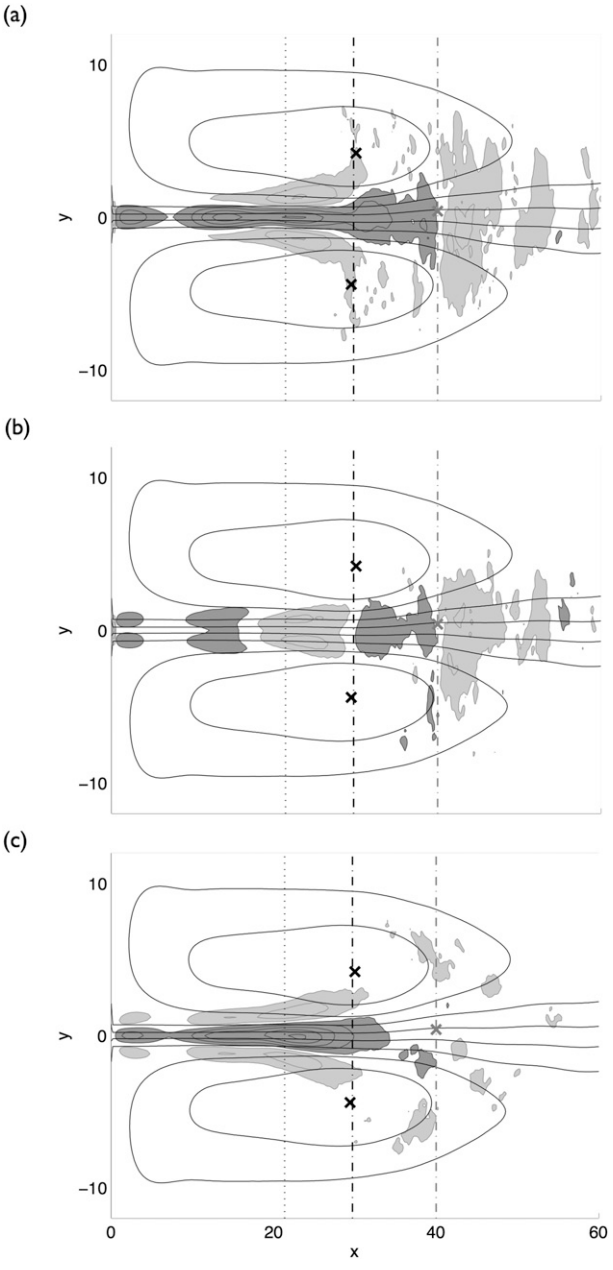

FIG. 11. The relative contribution of patterns of M and N to the full E vector divergence: (a) the total E vector divergence $\mathbf{V}\cdot\mathbf{E} = -2M_x - N_y$ and the individual contributions of (b) M $(-2M_x)$ and (c) N $(-N_y)$. Contours are drawn in intervals of 0.005 nondimensional units in all panels. Again note that upstream of $x = 10$, the dynamical balance is strongly influenced by sponge layer effects.

weakening of the mean jet to $x^{\mathrm{EKE\ max}}$, and helps drive the recirculations in the downstream region.

Advantages of the E vector perspective is its smoothness and simple dependence on M and N, its qualitative information on group velocity, and the direct visualization (through its divergence) of mean flow forcing in regions of strong zonal advection. In weaker flow regions, the mean flow forcing requires a vorticity equation interpretation of this divergence.

d. A mean streamline perspective

Further insight into the role of eddy forcing may be gained by consideration of the vorticity budget along mean flow streamlines. This view has the advantage of eliminating the effect of mean flow advection in the vorticity balance, which can obscure the role of the net eddy effect when viewing the eddy vorticity forcing as a time-mean Eulerian field. A consideration of the role of eddy forcing and the relative roles of M and N from this perspective for a streamline that remains inside the jet and for one inside the time-mean recirculation is summarized in Fig. 12.

Consider first the evolution of time-mean vorticity and the role of the eddy vorticity forcing along the jet (Fig. 12a–c). We note that here that the eddy vorticity forcing (the full time-mean eddy vorticity flux convergence approximated in Figs. 12c,f as $2M_{xy} + N_{yy}$) is everywhere negative upstream of $x^{\mathrm{EKE\ max}}$. Through the balance $\Delta\overline{\zeta}_a = -\beta\Delta y + \int(\text{eddy vorticity forcing})\mathbf{u}\cdot\delta\mathbf{l}$, where $\overline{\zeta}_a$ is the mean absolute vorticity consisting of the sum of relative and planetary components and the integral is taken along the path of a time-mean streamline, this will force a decrease in the absolute vorticity along the streamline path, consistent with the rapid decrease of $\overline{\zeta}_a$ seen upstream of the EKE maximum (Fig. 12b). A breakdown of the absolute vorticity into its relative and planetary components shows that here the eddy forcing acts primarily to decrease the relative vorticity with increasing distance downstream, thus removing much of the large relative vorticity associated with the jet shear upstream of x^*. Downstream of $x^{\mathrm{EKE\ max}}$, the eddy forcing is small but positive. Accordingly, the absolute vorticity increases slowly along the streamline. The relative vorticity continues to decrease but here, in the neutral wave radiator regime, decreasing relative vorticity is traded for increasing planetary vorticity and the jet broadens. A similar role of wave radiation in broadening the jet is pointed out by Mizuta (2012).

By considering the role of M versus N in the eddy forcing in this picture (Fig. 12c) we see that, consistent with previous diagnostics, the upstream effects forcing a decrease in the jet's relative vorticity are achieved largely by N_{yy} upstream of x^*. Again we see, however, that here M_{xy} plays a nonnegligible role. In the region where M is maximized on the jet flanks ($12 \lesssim x \lesssim 24$), M_{xy} acts to partially offset the effects of N_{yy} in the upstream region, and just downstream of x^*, forcing from M_{xy} replaces that from N_{yy} in supplying the majority of

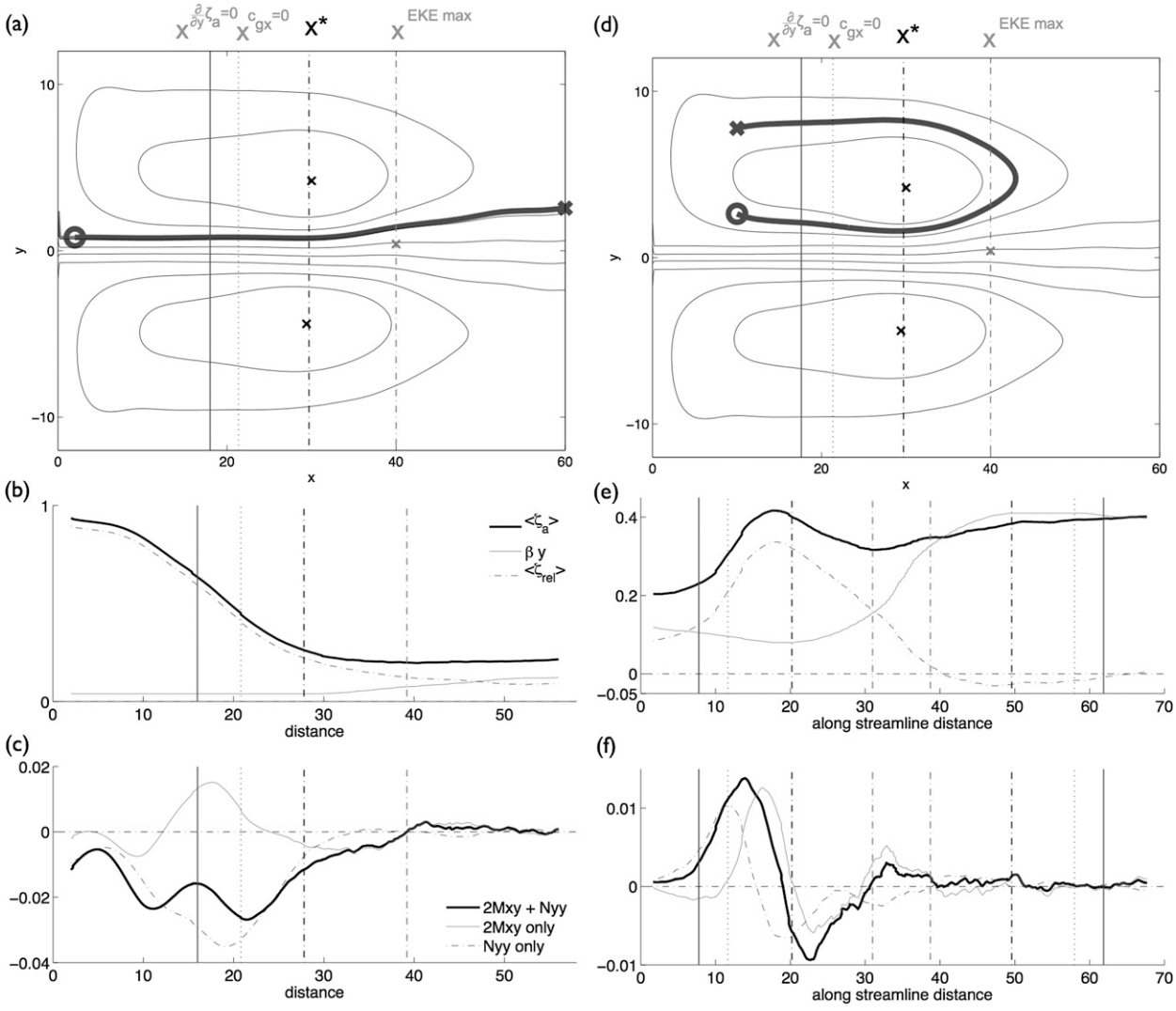

FIG. 12. A consideration of the role of eddy forcing and the relative roles of M and N in that forcing in the evolution of the time-mean vorticity (a)–(c) along the jet and (d)–(f) inside the recirculations. The along-streamline evolution of the time-mean vorticity (absolute vorticity and its relative and planetary constituents; middle panels) and the sense and strength of the eddy vorticity forcing (the time-mean eddy vorticity flux convergence and the relative contributions from gradients in M and N; bottom panels) along the streamlines highlighted in the top panels. Vertical lines denote important along-jet boundaries as indicated: solid gray denotes a local (along streamline) stability boundary [where $(d/dy)\overline{\zeta}_a$ becomes positive], dotted gray denotes the boundary between upstream and downstream eddy propagation inside the jet (where $c_{gx} = 0$), dash–dotted black indicates the along-stream location of x^*, and dash–dotted gray indicates the along-stream location of $x^{\mathrm{EKE\ max}}$.

the negative eddy vorticity forcing that acts to decrease $\overline{\zeta}_a$ along the streamline. In the far downstream region ($x \geq x^{\mathrm{EKE\ max}}$), M_{xy} is solely responsible for the positive eddy vorticity forcing and as such the broadening of the jet downstream.

The picture along a streamline inside a time-mean recirculation (Fig. 12d–f) differs in some important ways, underpinned by important differences in the along-stream evolution of $\overline{\zeta}_a$. As seen in Fig. 12e, the time-mean vorticity first increases along the jet to a local stability boundary as relative vorticity is fluxed from the jet core to the jet flanks. It then decreases along the jet in a local ''stable'' regime, and then increases again downstream of the EKE maximum as a parcel on the mean streamline moves northward and cyclonically in its ''turning of the corner'' on the downstream edge of the gyre (Fig. 12d). The sign of the eddy vorticity forcing changes in line with the changing tendency for $\overline{\zeta}_a$. In contrast to inside the jet, the eddy vorticity forcing is largely positive in the upstream region. Also in contrast to inside the jet, here both

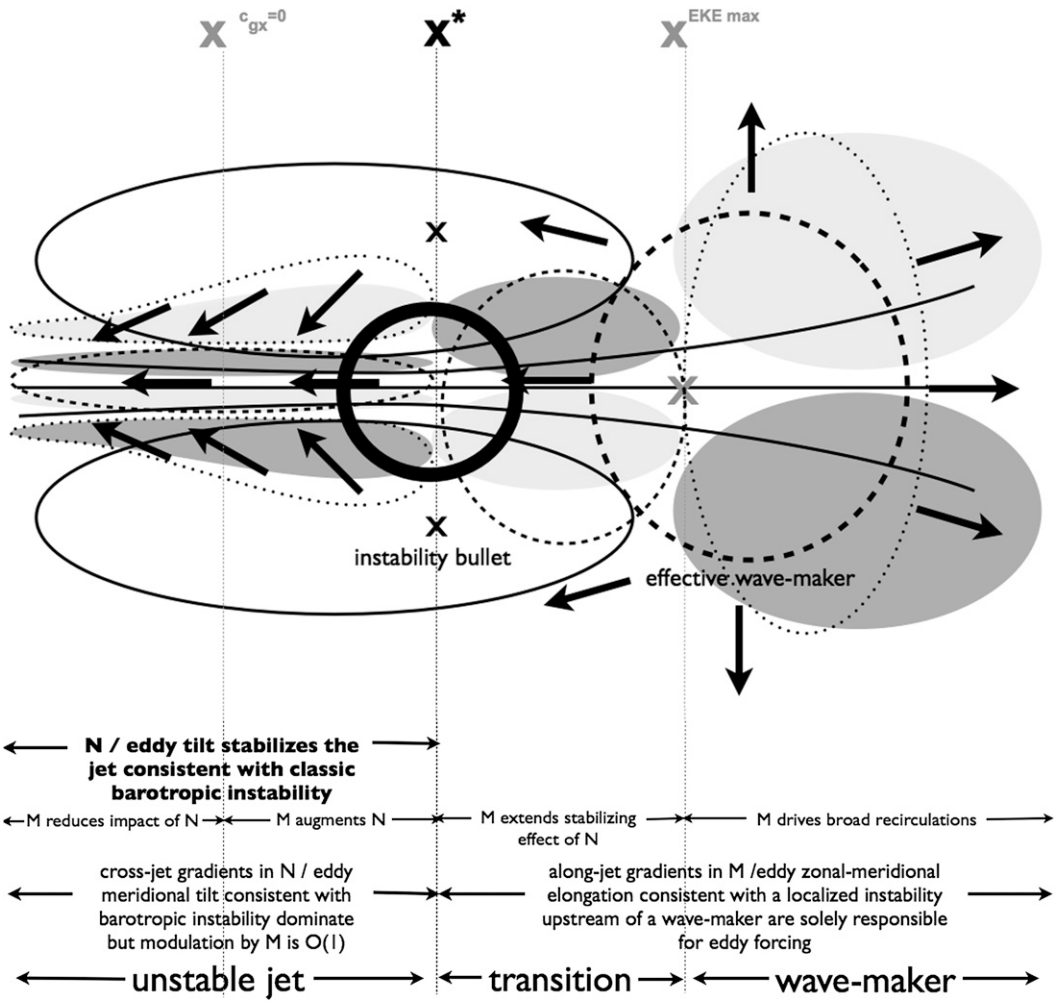

FIG. 13. A schematic summary of eddy–mean flow feedback effects and their relation to key features of the time-mean circulation and conceptualizations of the workings of the system. Filled contours are a schematic representation of the time-mean eddy vorticity flux convergence. Black arrows are a schematic representation of the E vectors, and black dashed and dotted contours are key features of the E vector convergence (dashed lines denote positive values, that is, an E vector convergence while dotted lines denote negative values, an E vector divergence).

N_{yy} and M_{xy} provide a positive forcing and play order-one roles, with M_{xy} again responsible for pushing the upstream region's extent further downstream. This along-streamline view shows how this upstream eddy forcing enables the time-mean recirculations to develop a broad meridional extent: the increase in relative vorticity supplied by M and N upstream of the local stability boundary is traded back for planetary vorticity further downstream all the way to the northern extent of the recirculation. The positive eddy vorticity forcing downstream of the EKE maximum also enables mean meridional motions and the development of cyclonic circulation required to close the recirculations at their downstream edge. This latter effect arises from contributions from M alone, which overcomes the opposite-signed forcing from gradients of N.

In summary (Fig. 13), a consideration of the eddy–mean flow feedback in terms of the individual contributions arising from the terms of the anisotropic part of the horizontal velocity correlation tensor, M and N, links various eddy effects in the various regimes of the flow with the spatial patterns of the two components of eddy elongation, respectively. The consideration of various diagnostics of the eddy–mean flow feedback described above give a consistent picture as follows. In the upstream unstable jet regime, eddy forcing is dominated from effects arising from the cross-jet patterns of N/meridional eddy tilts that act to stabilize the jet consistent with the

classical picture of barotropic instability. Contributions from M/eddy zonal–meridional elongation here, however, have an order-one modulating effect, reducing the stabilizing effect of N in the near field close to the western boundary and augmenting the stabilizing effect of N in the vicinity of x^*. Downstream eddy forcing arises almost exclusively from patterns in M/eddy zonal–meridional elongation, and acts to extend the region in which the mean jet is weakened and eddy energy is increased further downstream, as well as to drive the time-mean recirculations. This downstream-forcing pattern can be conceptualized as resulting from an along-jet evolution of eddy zonal–meridional elongation consistent with a localized instability at x^* upstream of an effective wave maker centered on the jet axis in the vicinity of $x^{\mathrm{EKE\ max}}$. The pattern of the E vector flux closely mirrors that of wave propagation, being toward the jet and upstream in the upstream unstable jet region and away from the effective wave radiator in the vicinity of $x^{\mathrm{EKE\ max}}$, and the interpretation of the divergence of this field as an effective eddy zonal force gives a consistent picture of the eddy forcing in the regions of strong zonal flow. Elsewhere, and in particular at the eastern edges of the time-mean recirculations, the E vector divergence is better understood as leading to mean flow away from the axis, thus acting to advect planetary vorticity which balances the mean vorticity generation associated with the meridional gradient of the E vector divergence.

6. Summary and discussion

In summary, we have revisited a study of eddy–mean flow interactions in an idealized model of a WBCE jet by considering the spatial patterns of terms of the time-mean horizontal velocity correlation tensor, K, M, and N, that together have implications for the spatial patterns of average eddy shape, orientation, propagation, and mean flow feedback. The aim has been to link the observed eddy effects in this configuration to eddy properties, and, through this association, potentially gain new insights into the physical mechanisms underpinning the eddy–mean flow interactions observed.

Our study shows that the idealized WBCE jet is characterized by a broad distribution of eddy kinetic energy K centered around a downstream maximum consistent with wave radiation from the jet downstream of the time-mean jet's stability boundary at x^*. The components of a two-dimensional description of eddy elongation, M and N, are characterized by large and positive M values in the upstream region, negative M values in the ''bullet of instability'' in the vicinity of x^*, and both positive and negative M values in the downstream region consistent with the existence of an effective wave maker centered on the jet axis in the vicinity of $x^{\mathrm{EKE\ max}}$. Here, N values are consistent with the signatures of barotropic instability in the upstream ''unstable'' jet region and wave radiation in the downstream wave radiator region. These distributions imply that on average eddies inside the jet are locally highly anisotropic and oriented zonally in the upstream region, circular in the vicinity of x^* and $x^{\mathrm{EKE\ max}}$, and increasingly anisotropic and oriented meridionally further downstream. On the flanks of the unstable jet and in the far field, eddies are anisotropic and tilted into the shear and with the shear respectively. These distributions also suggest that on average wave propagation inside the jet can be near zero or even negative upstream of $x^{c_{gx}=0}$. This is consistent with zonally elongated eddy activity continuing to exist in this region rather than being swept downstream by the jet. In the far field, wave radiation is away from the effective wave maker at $x^{\mathrm{EKE\ max}}$. The existence of the bullet of instability, the region of anomalous properties in the vicinity of x^*, remains a slight enigma in terms of our interpretations, which are derived from linear, neutral wave dynamics, though the eddy feedback arguments below may be sufficient.

By considering the eddy–mean flow feedback effects in terms of the anisotropic horizontal velocity correlation tensor terms, M and N, and using a number of perspectives, we associate various eddy effects with spatial patterns of eddy elongation characteristics. In the idealized model considered here, this exercise confirms our expectation of the stabilizing effects of eddies in the upstream region, and shows that it arises largely from cross-jet patterns in N/meridional eddy tilt. It also however gives new insight into additional eddy forcings that arise primarily from along-jet patterns in M/eddy zonal–meridional elongation. Close to the western boundary (where eddy anisotropy is extreme and wave propagation is upstream on the flanks of the jet) the eddy forcing arising from M reduces and modulates the stabilizing effect of N. However, in the vicinity of x^*, it augments then extends stabilizing effects of N and drives mean meridional motions. Finally, in the downstream wave radiator region, it acts to help close the broad recirculation gyres downstream of the EKE maximum. The existence of the instability bullet is crucial in extending the region of jet broadening downstream beyond the zone of classic barotropic instability. It is therefore consistent that there is eddy growth in this region. It is significant to note that the eddy-driven mean flow outside the unstable jet region arises predominantly from the M contribution to the eddy forcing and thus depends on the zonal–meridional elongation of eddies.

One way in which the consideration of the eddy forcing from this perspective based on spatial patterns of

average eddy shape and orientation characteristics can be helpful is through its potential to suggest, through the identification of the physical mechanisms that give rise to the distributions of eddy shape and orientation characteristics, the physical mechanisms that underpin various aspects of the eddy-forcing effect. The resulting mechanism-based understanding of the eddy forcing can then be applied to understanding where and when the various eddy effects arise, and may suggest the essential ingredients for parameterization of these impacts. In the idealized model considered here, the various diagnostics of the eddy effects discussed in section 5 consistently reveal that the pattern of deceleration at the jet axis and acceleration at the jet flanks in the upstream region arises primarily from a cross-jet pattern of N in which, consistent with the jet's instability, eddies lean against the shear and extract energy from the mean flow. In this way, one can attribute the stabilizing effect of eddies upstream of x^* to systematic patterns of eddy meridional tilts to the north and south of the jet arising from the jet's instability.

The physical mechanisms underpinning the key patterns of M, the consequent impact on the jet and, importantly, the driving of the time-mean recirculations, are less obvious, and instability modes relevant to the inflowing jet, their various growth rates relative to an advection time scale, wave radiation, and mean flow shear deformation are all likely playing a role in setting the downstream evolution of eddy zonal–meridional elongation characteristics. As discussed in section 5a, the forcing pattern arising from M in the downstream region can be understood as resulting from an instability signature of meridional elongation at x^* upstream of an effective wave maker downstream of $x^{\mathrm{EKE\ max}}$, with zonally elongated waves found westward and meridionally elongated waves found eastward of the effective wave maker location. Differences in the eddy-forcing patterns from a model of an isolated wave maker, however, suggest that additional physics may be at play, and the study of an isolated wave radiator model (see Waterman and Jayne 2012) suggests that eddy–wave interaction with the time-mean jet may be an important process to consider. Consistently, a consideration of the effects of the spatially varying mean flow, specifically the zonal-stretching deformation effects of the zonally evolving time-mean jet on the eddy shape properties as they propagate, as outlined below, predicts several trends in the along-stream evolution of eddy elongation consistent with that observed. As such, we suggest that the consideration of this influence may offer useful insight.

To consider the effects of Doppler shifting resulting from the mean jet structure on the along-stream evolution of eddy elongation, consider first the kinematic theory of Rossby wave trains in a spatially varying mean flow (see Lighthill 1977; Hoskins and Karoly 1981) and exploit the conservation of a wave's Doppler-shifted frequency $\omega_D = \omega_{\mathrm{intrinsic}} + \overline{\mathbf{U}} \cdot \mathbf{k}$, following a wave packet. [Here, $\overline{\mathbf{U}}$ is the mean (background) flow velocity and $\mathbf{k}$ is the eddy wavenumber vector.] The invariance of ω_D along a ray path implies that if $\overline{\mathbf{U}}$ changes along a ray, $\mathbf{k}$ must change at a rate of change that depends on the wavenumber and the rate of change of $\overline{\mathbf{U}}$ in space. Intuition can come from considering the simple case of a wave propagating along the jet axis such that the background flow can be considered to be purely zonal with $d\overline{U}/dy = 0$. In this case, with the usual assumptions of separation in the scales of the wave and background flow, the rate of change of k along a ray is then given by $Dk/Dt = -k(d\overline{U}/dx)$. Thus in regions of negative-stretching deformation, $d\overline{U}/dx < 0$, the wave will decrease its zonal scale (i.e., increase its wavenumber k) to conserve its Doppler-shifted frequency, while conversely in regions of positive-stretching deformation, $d\overline{U}/dx > 0$, it will increase its zonal scale (i.e., decrease its wavenumber k). The corresponding change in the meridional scale/l wavenumber may then be determined by exploiting the conservation of frequency following the wave packet.

Consider next the evolution of Rossby wavenumbers for a propagating wave inside the jet because of interaction with the observed zonal flow via a ray-tracing thought exercise as outlined in appendix B. For waves on the flanks of the jet in the upstream region ($x < x^{c_{gx}=0}$), where propagation is upstream and $d\overline{U}/dx > 0$, the influence of positive-stretching deformation of the downstream-accelerating jet on the upstream-propagating wave results in a decrease in k as the eddy–wave propagates. Eddy zonal–meridional elongation, $M \sim l^2 - k^2$, increases, and eddies become more and more zonally elongated as they approach the western boundary. The zonal distribution of decreasing M with increased distance from the boundary that results leads to $M_x > 0$: eddies decelerate the jet on its flanks thus acting to sharpen the jet. In contrast, in the downstream region ($x > x^{d\overline{U}/dx=0}$) eddies propagate downstream and $d\overline{U}/dx < 0$. The negative-stretching deformation of the decelerating jet on the downstream-propagating waves now predicts an increase in k along the ray path with distance downstream. Here, M decreases in concert resulting in the negative values of M_x that underpin the downstream eddy jet acceleration.

In short, both the eddy-sharpening effect (underpinned by $M_x > 0$) in the near-field upstream region ($x < x^{c_{gx}=0}$) and the eddy acceleration of the jet (underpinned by $M_x < 0$) in the downstream region ($x > x^{\mathrm{EKE\ max}}$) are consistent with the prediction for the evolution of eddy zonal–meridional elongation that would arise from the

effects of Doppler shifting on the eddy wavenumbers as they propagate. We further note (see Fig. 6) that the downstream maxima of EKE aligns with the region of maximum negative-stretching deformation, $d\overline{U}/dx < 0$, consistent with the accumulation of wave activity that would occur as a result of gradients in the mean flow forcing a convergence of the eddy–Rossby wave mode's group characteristics, with modes with initially eastward Doppler-shifted group speeds (i.e., shorter modes) trapped in the negative deformation region (see Webster and Chang 1988; Chang and Webster 1990, 1995). In these ways, the zonal evolution of the mean jet structure, characterized by acceleration upstream of x^* and rapid deceleration centered at $x^{\mathrm{EKE\ max}}$, may play an important role in determining the average along-stream evolution of eddy elongation from zonal elongation upstream to meridional elongation downstream, as well as in the accumulation of wave energy in the downstream maximum that also has important influences on the patterns that determine the eddy effects. It should be noted that the application of ray-tracing theory here involves several approximations and caveats, and in some places such as the upstream region where the jet is unstable, the scale of the waves is comparable to that of the variations of the mean flow, and nonlinear interactions are likely important, we apply the theory outside its domain of strict applicability. Further, it is only one of several processes inside the jet that may be important in setting the along-stream evolution of eddy shape and orientation properties. Despite this, however, there are many reasons to believe that the predictions based on these simple ideas remain valuable in predicting many aspects of the observed behavior and in offering a physical feel for the dynamics at play.

In closing, we note that the perspective obtained in this paper on the eddy forcing can also be useful in providing an understanding of its dependence on various eddy properties, and as such may help to explain why the mean flow–driving effect of eddies breaks down as the spatial resolution of the model computation is degraded. A key result of this study is the new insight into the important role that the along-jet evolution of eddy shape, and in particular eddy zonal–meridional elongation, can play in the eddy forcing in both the up- and downstream regions. It acts to extend and strengthen the WBCE, and it determines the nature and strength of the recirculations. This understanding suggests that the failure to adequately resolve eddy elongation properties could underlie the deficiencies seen in these mean flow properties in this idealized model for reduced spatial resolutions. A subsequent paper will explore this topic. This understanding can further be applied to the task of suggesting new ideas for the parameterization of unresolved eddy effects. An obvious one suggested by this work is parameterization in terms of eddy shape and orientation characteristics, potentially exploiting the strong connection between eddy orientation and stability theory. For a discussion of work in this direction, see Marshall et al. (2012). The potential to exploit the perspective on the eddy forcing gained here in parameterization design will also be a topic of future work.

Acknowledgments. The authors would like to gratefully acknowledge useful discussion with Steven Jayne, Jonathan Lilly, David Marshall, and James Maddison. SW acknowledges the support of the U.K. Natural Environmental Research Council (NERC) (Grant NE/G001510/1), as well the Australian Research Council (ARC) (Grant RM10240) and the ARC Centre of Excellence for Climate System Science (Grant CE110001028).

APPENDIX A

Damped Eddy-Forcing Experiments

The goal of the eddy-forcing experiments is to diagnose the mean circulation driven by the eddy forcing in the form of the time-mean eddy vorticity flux convergence or individual components of that quantity diagnosed from a standard model run and applied as a forcing term on the right-hand side of the time-evolving quasigeostrophic potential vorticity (QGPV) equation, which governs the system dynamics. To preserve the background/time-mean jet effects, namely strong mean zonal advection and a contribution to the background time-mean vorticity gradient found to be important in clarifying the interpretation of eddy-forcing experiment results, in these experiments the same jet inflow and outflow as the standard run is maintained. To prevent a contribution to the net eddy forcing by the eddies associated with the jet's instability (and thus restrict the eddy forcing in the system to only the parameterized eddy forcing prescribed on the governing equation's right-hand side) all eddies in the system are damped by means of what is in essence a time filter. The filter is achieved by computing the time evolution of a filtered PV field q_{filtered}, which evolves in time in part according to QGPV dynamics forced by the prescribed static parameterized eddy forcing and in part according to the evolution of a slowly evolving PV variable q_{slow} that damps changes to q_{filtered} on fast time scales. In this way, eddy effects associated with short time scales, say those associated with the inflowing jet's instability, can be damped while the influences of the prescribed eddy forcing, which has an infinite time scale, are accumulated and

incorporated into the evolution of the filtered field over a long-time integration.

The practical implementation of the filter is as follows. At each time step $t = n$.

(i) We compute the change in PV predicted by the QGPV equation forced by the prescribed eddy forcing on its right-hand side: $dq(t = n) = dt\{-J[\psi(t = n - 1), \zeta(t = n - 1)] + \beta y + (\text{the eddy forcing}) - R\zeta(t = n - 1)\}$.

(ii) We update q_{filtered} by this change in q: $q_{\text{filtered}}(t = n) = q_{\text{filtered}}(t = n - 1) + dq(t = n)$.

(iii) We next update a second "slowly evolving" q variable q_{slow} computed as the weighted sum of the newly updated q_{filtered} at this time step (i.e., evolving according to the static eddy–forced QGPV dynamics) and the slowly evolving q at the previous time step: $q_{\text{slow}}(t = n) = [1 - \epsilon]q_{\text{slow}}(t = n - 1) + \epsilon q_{\text{filtered}}(t = n)$, where square brackets indicate an index that is not a time step. In this way, q_{slow} incorporates eddy effects only on slowly evolving time scales with the weighting factor ϵ selecting which time scales are damped. In the limit $\epsilon = 0$, q_{slow} is unchanging in time and remains fixed at its initial value (i.e., all time scales are damped). In the limit $\epsilon = 1$, $q_{\text{slow}} = q_{\text{filtered}}$ and all time scales are passed. As ϵ is increased from 0 to 1, more and more higher-frequency motions are included in the slowly evolving q variable. Here, ϵ defines the damping time scale of q_{slow}, which can be shown to be given by $R\Delta t$ where $R = -1/\ln(1 - \epsilon)$ and Δt is the model time step.

(iv) We go back and modify q_{filtered} at this time step by replacing it with a weighted sum of q_{filtered} computed in step (ii) (i.e., evolving according to the full QGPV equation dynamics forced by the prescribed eddy forcing) and q_{slow} computed in step (iii): $q_{\text{filtered}}(t = n) = q_{\text{filtered}}(t = n)|_{\text{from step (ii)}} - A[q_{\text{filtered}}(t = n)|_{\text{from step (ii)}} - q_{\text{slow}}(t = n)|_{\text{from step (iii)}}] = [1 - A]q_{\text{filtered}}(t = n)|_{\text{from step (ii)}} + Aq_{\text{slow}}(t = n)|_{\text{from step (iii)}}$, where square brackets indicate an index that is not a time step. The damping strength A controls the relative influence of the forced QGPV dynamics-evolving q field versus the slowly evolving q field on the filtered q variable. As such, for sufficiently large damping strengths, the filtered q field does not contain significant eddy motion on time scales less than and equal to the damping time scale, and it is forced by eddies only on longer time scales and the static eddy forcing applied to the governing equation's right-hand side.

(v) Finally, we invert q_{filtered} computed above [in step (iv)] to find the streamfunction at this time step, $\psi(t = n)$. It is the vorticity associated with $q_{\text{filtered}}(t = n)$ [computed in step (iv)] and $\psi(t = n)$ [computed here in step (v)] that are used in the QGPV equation in step (i) for time step $t = n + 1$.

For our purposes here we wish to select values of ϵ and A that produce a smooth (eddy free) field with a time-mean circulation that, in the absence of any right-hand side forcing, is free of eddy-driven effects such as the time-mean recirculation gyres and along-stream modifications to time-mean jet strength. To determine these values, we performed a series of tests with no eddy forcing prescribed varying ϵ over four orders of magnitude [corresponding to damping time scales ranging from O(0.1 days) to O(1000 days)] and varying A between 0 and 1. Results of these tests determined choice values of ϵ and A of $\epsilon = 1/10\,000$ [corresponding to a damping time scale of O(300 days)] and $A = 9/10$, as these values produced a filtered q field with the signature of a strong (unstable) jet (in the upstream region) but no jet meandering or far-field wave radiation. It is on this background field that the effects of a prescribed eddy forcing were diagnosed.

We note that a damped forcing experiment applying the total eddy forcing (not shown) yields a mean circulation similar to that of the sum of those from the individual components, however, when compared with the actual mean circulation for the standard (unforced and undamped) configuration, eddy-driven recirculations in these experiments do not extend westward of the downstream location where they are forced (downstream of $x^{\text{EKE max}}$) in the same way as in the standard configuration. We hypothesize that Rossby wave propagation is responsible for transmitting the signal westward which is damped in our forcing experiments, and work toward understanding the dependence of the eddy effects realized as a function of damping time scale is ongoing.

APPENDIX B

Ray-Tracing Calculations

We consider the evolution of a Rossby wave wavenumber resulting from wave interaction with the time-mean velocity gradients of the zonally evolving jet via a ray-tracing calculation for waves originating at a variety of starting points x_{start} along the jet axis. The calculation consists of forward stepping the evolution of the position of the wave packet in time, determined by mean flow advection and relative Rossby wave group propagation. The latter is determined by the eddy wavenumbers (defining the eddy elongation), which evolve according to the influence of the mean flow $\overline{U}$, its gradients, and the time-mean absolute vorticity

gradient in such a way as to conserve wave frequency along the ray path. The calculation consists of the following steps.

(i) We set the initial wavenumber components k and l at $x = x_{\text{start}}$ and $y \sim 0$ to those diagnosed from the time-mean $\overline{\psi'\psi'}$, $\overline{u'u'}$, and $\overline{v'v'}$ fields via $k_1 = \sqrt{\overline{v'v'}/\overline{\psi'\psi'}}$ and $l_1 = \sqrt{\overline{u'u'}/\overline{\psi'\psi'}}$.[4]

(ii) We use the initial wavenumber components and local $\overline{U}$ and $(\partial/\partial y)\overline{\zeta_a}$ values to also define the initial zonal wave group velocity, again assuming that locally the linear Rossby wave dispersion relation applies:

$$c_{gx1} = \overline{U}(x_{\text{start}}, 0) + \frac{\partial}{\partial y}\overline{\zeta_a}(x_{\text{start}}, 0)\frac{k_1^2 - l_1^2}{(k_1^2 + l_1^2)^2}. \quad \text{(B1)}$$

Note throughout the calculation we assume strictly zonal wave propagation.

(iii) We next step forward the wave's zonal position and wavenumber. These evolve because of mean flow advection, intrinsic wave propagation, the influence of the background flow gradient, $d\overline{U}/dx$, and changing background $\overline{U}$ and $(\partial/\partial y)\overline{\zeta_a}$ values. At each time step we compute:

- the new zonal position for the wave: $x_{n+1} = x_n + dx_{n+1}$ where $dx_{n+1} = c_{gxn}\Delta t$
- the background flow gradient over the wave's displacement: $d\overline{U}/dx = [\overline{U}(x_{n+1}, 0) - \overline{U}(x_n, 0)]/(x_{n+1} - x_n)$
- the new zonal wavenumber that deforms in response to the background flow's zonal gradient: $k_{n+1} = k_n + (Dk/Dt)\Delta t$ where $Dk/Dt = -k_n(d\overline{U}/dx)$
- the new meridional wavenumber that changes in concert to conserve the wave's total frequency along the ray path (from a rearrangement of the Rossby wave dispersion relation):

$$l_{n+1} = \sqrt{\frac{\overline{U}(x_{n+1}, 0)k_{n+1}^3 - \omega k_{n+1}^2 - \frac{\partial}{\partial y}\overline{\zeta_a}(x_{n+1}, 0)k_{n+1}}{\omega - k_{n+1}\overline{U}(x_{n+1}, 0)}} \quad \text{(B2)}$$

- the new zonal group velocity that changes in response to changes in k, l, $\overline{U}$, and $(\partial/\partial y)\overline{\zeta_a}$:

$$c_{gxn+1} = \overline{U}(x_{n+1}, 0) + \frac{\partial}{\partial y}\overline{\zeta_a}(x_{n+1}, 0)\frac{k_{n+1}^2 - l_{n+1}^2}{(k_{n+1}^2 + l_{n+1}^2)^2}. \quad \text{(B3)}$$

The calculation results in a time series of wave packet position and its zonal–meridional elongation (diagnosed from the relative sizes of the wavenumber components k and l) along the ray path. The calculation is terminated when the wave packet moves out of the domain of interest or the wavenumber l becomes imaginary.

[4] The ray-tracing calculation requires initial values for the neutral wavenumbers as a function of x, and for the purpose of our thought exercise we wish to consider "typical" values. We obtain these from the gradients of the time-mean streamfunction and velocity variances as specified, which indicate the horizontal scales of dominant motions, but note several caveats associated with this choice. First, strictly time-mean values do not define the relevant initial conditions that instead are instantaneous values set by the growing instability modes, nonlinear interactions, and time-dependent Rossby wave dynamics. Second, the wavenumbers obtained in this way may not correspond to the wavenumbers of the neutral wave in the upstream region where barotropic instability dominates. For these reasons, these initial conditions should be interpreted as conceptual and not exact. They are viewed as appropriate for our purposes here as qualitative results are not critically dependent on the wavenumber magnitudes. Further, we neglect the imaginary component of l, expected to be associated with the growing modes of the unstable jet (see, for example, Talley 1983) and in the subsequent calculation consider only the evolution of neutral waves and not growing unstable modes to which the ray-tracing theory does not apply. Because the imaginary part of the propagation speed tends to be small relative to the relative real-valued propagation speed, we expect neutral wave arguments to be useful in predicting many properties of the growing waves, however, in the upstream unstable jet region, strictly we apply the theory outside its domain of applicability (as well as neglect nonlinear interactions that likely are important here) and as such results in the upstream region should be treated with caution. Finally, we take the sign of l to be positive, but recognize that the neutral waves radiated from the jet will have both positive and negative values of l to the north and south of the jet axis, respectively, as is required for energy propagation away from their energy source (the meandering jet). Assuming a positive l implies that we consider waves to the south of the jet, but we expect waves with negative l to the north of the jet to behave equivalently.

REFERENCES

Adams, J., P. Swartztrauber, and R. Sweet, cited 1988: FISHPACK: Efficient FORTRAN subprograms for the solution of separable elliptic partial differential equations. [Available online at http://www.cisl.ucar.edu/css/software/fishpack.]

Arakawa, A., 1966: Computational design for long-term numerical integration of the equations of fluid motion: Part I: Two-dimensional incompressible flow. *J. Comput. Phys.,* **1,** 119–145.

Beliakova, N., 1998: Generation and maintenance of recirculations by Gulf Stream instabilities. Ph.D. thesis, Massachusetts Institute of Technology/Woods Hole Oceanographic Institute Joint Program, 224 pp.

Chang, H. R., and P. J. Webster, 1990: Energy accumulation and emanation at low latitudes. Part II: Nonlinear response to strong episodic forcing. *J. Atmos. Sci.,* **47,** 2624–2644.

——, and ——, 1995: Energy accumulation and emanation at low latitudes. Part III: Forward and backward accumulation. *J. Atmos. Sci.,* **52,** 2384–2403.

Dewar, W. K., and J. M. Bane, 1989: Gulf Stream dynamics. Part II: Eddy energetics at 73°W. *J. Phys. Oceanogr.,* **19,** 1574–1587.

Dingle, R. B., 1973: *Assymptotic Expansions: Their Derivation and Interpretation*. Academic Press, 521 pp.

Durran, D. R., 1991: The third-order Adams–Bashforth method: An attractive alternative to leapfrog time differencing. *Mon. Wea. Rev.,* **119,** 702–720.

Hogg, N. G., 1983: A note on the deep circulation of the western North Atlantic: Its nature and causes. *Deep-Sea Res.,* **30,** 945–961.

——, 1985: Evidence for baroclinic instability in the Gulf Stream recirculation. *Prog. Oceanogr.,* **14,** 209–229.

——, 1992: On the transport of the Gulf Stream between Cape Hatteras and the Grand Banks. *J. Mar. Res.,* **50,** 545–566.

——, 1993: Toward parameterization of the eddy field near the Gulf Stream. *Deep-Sea Res.,* **40,** 2359–2376.

Hoskins, B. J., and K. Karoly, 1981: The steady linear response of a spherical atmosphere to thermal and orographic forcing. *J. Atmos. Sci.,* **38,** 1179–1196.

——, I. N. James, and G. H. White, 1983: The shape, propagation, and mean flow interaction of large-scale weather systems. *J. Atmos. Sci.,* **40,** 1595–1612.

Howden, S. D., 2000: The three-dimensional secondary circulation in developing Gulf Stream meanders. *J. Phys. Oceanogr.,* **30,** 888–915.

Jayne, S. R., and N. G. Hogg, 1999: On recirculation forced by an unstable jet. *J. Phys. Oceanogr.,* **29,** 2711–2718.

——, ——, and P. Malanotte-Rizzoli, 1996: Recirculation gyres forced by a beta-plane jet. *J. Phys. Oceanogr.,* **26,** 492–504.

Kirtman, B. P., and Coauthors, 2012: Impact of ocean model resolution on CCSM climate simulations. *Climate Dyn.,* **39,** 1303–1328.

Lighthill, J., 1977: *Waves in Fluids.* Cambridge University Press, 504 pp.

Marshall, D. P., J. R. Maddison, and P. S. Berloff, 2012: A framework for parameterizing eddy potential vorticity fluxes. *J. Phys. Oceanogr.,* **42,** 539–557.

Mizuta, G., 2010: Rossby wave radiation from an eastward jet and its recirculations. *J. Mar. Res.,* **67,** 185–212.

——, 2012: Role of the Rossby waves in the broadening of an eastward jet. *J. Phys. Oceanogr.,* **42,** 476–494.

Morrow, R., R. Coleman, J. Church, and D. Chelton, 1994: Surface eddy momentum flux and velocity variances in the Southern Ocean from *Geosat* altimetry. *J. Phys. Oceanogr.,* **24,** 2050–2071.

Preisendorfer, R. W., 1988: *Principal Component Analysis in Meteorology and Oceanography.* Elsevier, 425 pp.

Qiu, B., 2000: Interannual variability of the Kuroshio Extension system and its impact on the wintertime SST field. *J. Phys. Oceanogr.,* **30,** 1486–1502.

Shay, T. J., J. M. Bane, D. R. Watts, and K. L. Tracey, 1995: Gulf Stream flow field and events near 68°W. *J. Geophys. Res.,* **100** (C11), 22 565–22 589.

Simmons, A. J., and B. J. Hoskins, 1979: The downstream and upstream development of unstable baroclinic waves. *J. Atmos. Sci.,* **36,** 1239–1254.

Spall, M. A., 1994: Wave-induced abyssal recirculations. *J. Mar. Res.,* **52,** 1051–1080.

——, 1996: Dynamics of the Gulf Stream/deep western boundary current crossover. Part II: Low-frequency internal oscillations. *J. Phys. Oceanogr.,* **26,** 2169–2182.

Starr, V. P., 1968: *Physics of Negative Viscosity Phenomena.* McGraw-Hill, 256 pp.

Talley, L. D., 1983: Radiating barotropic instability. *J. Phys. Oceanogr.,* **13,** 972–987.

Thompson, R. O. R. Y., 1978: Reynolds stress and deep countercurrents near the Gulf Stream. *J. Mar. Res.,* **36,** 611–615.

Throncroft, C. D., B. J. Hoskins, and M. E. McIntyre, 1993: Two paradigms of baroclinic-wave life-cycle behaviour. *Quart. J. Roy. Meteor. Soc.,* **119,** 17–55.

Waterman, S., and S. R. Jayne, 2011: Eddy–mean flow interactions in the along-stream development of a western boundary current jet: An idealized model study. *J. Phys. Oceanogr.,* **41,** 682–707.

——, and ——, 2012: Eddy-driven recirculations from a localized, transient forcing. *J. Phys. Oceanogr.,* **42,** 430–447.

——, N. G. Hogg, and S. R. Jayne, 2011: Eddy-mean interaction in the Kuroshio Extension region. *J. Phys. Oceanogr.,* **41,** 1182–1208.

Watts, D. R., K. L. Tracey, J. M. Bane, and T. J. Shay, 1995: Gulf Stream path and thermocline structure near 74°W and 68°W. *J. Geophys. Res.,* **100** (C9), 18 291–18 312.

——, X. Qian, and K. L. Tracey, 2001: Mapping abyssal current and pressure fields under the meandering Gulf Stream. *J. Atmos. Oceanic Technol.,* **18,** 1052–1067.

Webster, P. J., and H. R. Chang, 1988: Energy accumulation and emanation regions at low latitudes: Impacts of a zonally varying basic state. *J. Atmos. Sci.,* **45,** 803–829.